Coordination Chemistry Reviews 505 (2024) 215693

Contents lists available at ScienceDirect

Coordination Chemistry Reviews

journal homepage: www.elsevier.com/locate/ccr

Review

Advances of carbon nitride based atomically dispersed catalysts from single-atom to dual-atom in advanced oxidation process applications

Jie Deng [a], Yuxi Zeng [a], Eydhah Almatrafi [b], Yuntao Liang [a], Zihao Wang [a], Ziwei Wang [a], Biao Song [a], Yanan Shang [c], Wenjun Wang [d], Chengyun Zhou [a,b,*], Guangming Zeng [a,b,*]

[a] College of Environmental Science and Engineering and Key Laboratory of Environmental Biology and Pollution Control (Ministry of Education), Hunan University, Changsha 410082, China
[b] Center of Research Excellence in Renewable Energy and Power Systems, Center of Excellence in Desalination Technology, Department of Mechanical Engineering, Faculty of Engineering-Rabigh, King Abdulaziz University, Jeddah 21589, Saudi Arabia
[c] School of Safety and Environmental Engineering, Shandong University of Science and Technology, Qingdao 266590, China
[d] School of Resources and Environment, Changsha Social Laboratory of Artificial Intelligence, Hunan University of Technology and Business, Changsha 410205, China

ARTICLE INFO

Keywords:
Graphitic carbon nitride
Atomically dispersed catalysts
Advanced oxidation process
Environmental application

ABSTRACT

Single-atom catalysts are an essential research object in environmental catalysis because of their unique coordination environment, high utilization rate, high activity and selectivity. The dual-atom catalysts have two sets of atomic centers. The atomically dispersed catalysts (ADCs) from single-atom to dual-atom can bridge the gap between heterogeneous and homogeneous catalysts. The key to the ADCs is forming a stable metal single-atomic site between the catalyst and the support. Graphite carbon nitride has the advantages of chemical stability, structural regulation and visible light absorption. It is one of the most promising two-dimensional materials for stabilizing isolated metal atoms. As an advanced heterogeneous catalyst, graphitic carbon nitride (g-C_3N_4) based ADCs have great potential in applying advanced oxidation processes (AOPs) to solve environmental problems. However, the research progress of g-C_3N_4 based ADCs in AOPs needs to be summarized more comprehensively. In this paper, the preparation, catalytic mechanism, stability analysis and environmental application of these materials are reviewed systematically. Finally, the research progress of g-C_3N_4 based ADCs and the prospects and challenges of this new field prospect are summarized.

1. Introduction

In recent years, with the rapid development of the economy and accelerating industrialization, chemical resources are constantly consumed, and environmental problems have arisen. The wastewater discharged from industrial and agricultural development contain many pollutants, which have a terrible effect on the ecological environment and human health [1,2]. The application of advanced oxidation processes (AOPs) to solve environmental problems has attracted extensive attention. These organic pollutants will be decomposed into small molecules or H_2O, CO_2 via an oxidation process based on multiple active species such as hydroxyl radical (•OH), sulfate radical ($•SO_4^{2-}$), superoxide radical ($•O_2^-$), single oxygen ($^1O_2$), high valence metal oxidizing species [3–5].

AOPs is a very efficient means to remove environmental pollutants [6,7]. Atomically dispersed catalysts (ADCs) have attracted extensive attention in the field of advanced oxidation due to its unique advantages such as high atomic utilization efficiency, high activity and excellent selectivity. ADCs include single atom catalysts (SACs), dual-atom catalysts (DACs), and clusters. The single metal site as the active center of SACs has been widely studied in the field of environmental catalysis. In addition, DACs has attracted extensive attention because of its two sets of metal sites with more abundant catalytic mechanisms [8]. Wang et al. prepared Ag single-atom catalysts (SACs) as a visible photocatalyst. When peroxymonosulfate (PMS) is present, Ag SACs can efficiently degrade bisphenol A (BPA) [9]. As an extremely reactive and stable Fenton-type catalyst, the Co SACs prepared by Li et al. effectively catalyze the oxidation of intractable organic matter through the activation of PMS [10]. In addition, Zeng et al. elucidated the conformational relationship and potential catalytic mechanism of Co-SACs in

* Corresponding authors at: College of Environmental Science and Engineering and Key Laboratory of Environmental Biology and Pollution Control (Ministry of Education), Hunan University, Changsha 410082, China.
E-mail addresses: zhouchengyun@hnu.edu.cn (C. Zhou), zgming@hnu.edu.cn (G. Zeng).

https://doi.org/10.1016/j.ccr.2024.215693
Received 18 October 2023; Accepted 21 January 2024

environmental catalytic applications [11]. Heterogeneous catalysts are widely used in environmental pollution control technology [12]. In the heterogeneous catalysis process, the catalyst interacts with the reactant at the active site on the solid surface. Improving the active component is the key to preparing high-quality catalysts. To downsize the active element to the single-atom scale, the SACs has a completely exposed surface metal atom with the maximum atomic utilization, and high catalytic activity [13,14]. The SACs can form chemical bonds with the primary material and construct a stable metal single-atomic site. The unsaturated coordination center, stable support and carbon matrix affect the catalytic efficiency of SACs [15]. Subsequently, DACs show a new development prospect in heterogeneous catalysis. DACs have two sets of single-atomic structures, and different monitors can play other functions in the catalytic reaction [16]. The collaboration between the two can improve the utilization rate of atoms and the catalytic efficiency and stability of the catalyst. The interaction force between the dual atoms and the strong interaction between the atoms and the substrate have richer performance in terms of the stability line, selectivity and activity of environmental catalysis [17]. DACs can show more advantages by modulating the chemistry of the substrate. In addition, DACs can complete some reaction pathways that SACs sometimes cannot, such as adsorption through multiple sites formed by bond breaks [18,19]. However, as the particle size of metal atoms decreases, the surface energy of the catalyst increases sharply and tends to form clusters. The underlying support plays a decisive role in affecting the structure–property relationship. Therefore, to anchor isolated metal atoms and create SACs, it is crucial to choose a support with a lot of binding sites and a strong enough bond.

Currently, the design of SACs based on N-rich carbon materials (i.e., MOFs, N-doped carbon nanotube, graphitic carbon nitride (g-C_3N_4), N-doped graphene) has a great application prospect [20,21]. There is a large number of N atoms in g-C_3N_4 that can trap metal atoms. Therefore, it is widely used to fix and support metal atoms. The carbon and nitrogen of g-C_3N_4 can form sp^2 hybridization, producing a highly conjugated electronic structure, resulting in a stable structure [22]. All these characteristics are conducive to the photo responsive applications of g-C_3N_4. There are great advantages for g-C_3N_4 in chemical stability, structural regulation and visible light absorption [23,24]. Recently, new heterogeneous catalysts made of carbon nitride based SACs have been employed in a variety of advanced oxidation systems, such as photocatalysis, photo/PMS, photo/H_2O_2, and Fenton-like processes, to degrade organic contaminants [25,26]. There are many successful examples of treating organic pollutants in water and other environmental and energy applications.

The current research on ADCs is progressing well, and the number of reviews is increasing [8,27,28]. Wang et al. reviewed the application progress of atomically dispersed materials (ADMs) in the fields of environmental catalysis, electrocatalysis and photocatalysis, and the opportunities and problems faced by ADMs in various reactions. Wu et al. discussed the advanced oxidation technology of SACs based on persulfate and the interaction mechanism of persulfate with SACs [29]. Lin et al. reviewed the synthesis, improvement and application of carbon nitride materials in the environment [30]. Singh et al. reviewed the role of SACs in organic conversion and energy conversion-related applications [31]. Liu et al. comprehensively elaborated the synthesis strategy and application of SACs as electrode materials in lithium-sulfur batteries for energy storage systems [32]. At present, there have been some researches on the application of DACs in AOPs [33,34]. Dong et al. studied the degradation of pollutants such as bisphenol A by constructing DACs to activate PMS. It was found that the degradation efficiency of the DACs was doubled compared with that of SACs. In addition, Wang et al. found that the DACs has significant catalytic activity in acidic and alkaline media, showing strong durability. However, there are only a few comprehensive reviews on the treatment of contaminants in aquatic environments by carbon nitride-based SACs and DACs in AOPs. Therefore, we can make a summary of the research in this area.

In this review, we first introduce carbon nitride to highlight the advantages of using carbon nitride as the SACs substrate. Secondly, the synthesis methods of SACs and DACs are summarized, including several common transition metal single-atom catalysts, especially the synthesis methods of g-C_3N_4 based DACs and their formation process and coordination environment are revealed. Thirdly, the innovative application of g-C_3N_4 based ADCs in environmental catalysis was emphasized to reveal the relationships between catalytic sites, reaction mechanisms and pollutant degradation processes of these catalysts in different advanced oxidation systems. In addition, the stability of these materials was analyzed. Finally, the opportunities and challenges of carbon nitride based atomically dispersed materials in environmental catalysis were proposed.

2. Synthesis of carbon nitride

The first synthesis of the polymer carbon nitride dates back to 1834 [35]. The non-metallic polymer carbon nitride has many advantages, and many scholars favor it regarding material source, chemical stability and structural regulation [36]. In 1996, some scholars proposed that carbon nitride has five different crystal structures, among which g-C_3N_4 is the most stable [37]. Because in this structure, carbon and nitrogen atoms undergo sp^2 hybridization, forming a highly conjugated structure similar to the benzene ring. Moreover, the basic construction of carbon nitride is composed of tri-s-triazine units. And studies have shown that carbon nitride based on such a structure has lower energy, is thermodynamically stable, and is more stable overall [38]. Nowadays, g-C_3N_4 are mainly plane structures formed by the connection of triazine structure and heptazine structure with nitrogen atom [39]. Such a structure can promote the dispersion and anchoring of metal single atoms, and the introduction of metal elements can reduce the band gap, which is conducive to charge transfer, thus increasing the catalytic activity [40]. g-C_3N_4 is metal-free, so the price is low, and the chemical stability is good, non-toxic, easy to synthesize [41,42]. Carbon nitride has a medium band gap of 2.7–2.8 eV and can absorb visible light of 450–460 nm, which is universal [43].

g-C_3N_4 is usually synthesized by thermal polymerization. Two steps make up the preparation process: polyaddition and polycondensation. Various nitrogen-containing organic compounds have been used as pyrolytic precursors, such as urea, thiourea, cyanamide, dicyandiamide, melamine, etc. The forms and properties of g-C_3N_4 prepared by different precursor systems are also different. Some studies have found that melamine or dicyandiamide as a precursor has a high yield and thermal stability [44]. Zhao et al. found early in 2005 that g-C_3N_4 prepared with melamine showed high thermal stability at high temperatures in thermogravimetry (TG) analysis [45]. In addition, it has been found that g-C_3N_4 prepared from urea has high catalytic activity. By comparing the properties of g-C_3N_4 prepared from different precursors (urea, thiourea, and dicyandiamide), Martin et al. found that g-C_3N_4 prepared from urea has a larger specific surface area, which improves charge separation and migration [46]. As for melamine as a precursor, it is heated until ammonia gas is generated, which causes a polycondensation reaction. Continue heating, g-C_3N_4 will generate. Yan et al. synthesized a g-C_3N_4 photocatalyst using low-cost melamine as raw material by direct heating [47]. In addition to the most common thermal polymerization, solid-state reactions, solvothermal synthesis, and liquid-phase electrodeposition techniques were applied to the synthesis of g-C_3N_4 [48–50]. The proportion and structure of g-C_3N_4 affect its thermochemical stability. When the C/N ratio gradually increases from 1 to 1.33, its catalytic or photocatalytic efficacy may also be impacted by the structure's crystallization transition from a more disordered phase to a graphite phase [51].

Wang et al. summarized preparation methods developed by g-C_3N_4 based on thermal polymerization, including templating methods, template-free methods, sol–gel methods, supramolecular preorganization methods, exfoliation methods and so on. Both soft and hard

templating techniques are used in templating. The soft template method is by the assembly of surfactant and inorganic phase to prepare g-C_3N_4. Zhao et al. used cyanuric acid and melamine to prepare hollow mesoporous g-C_3N_4 microspheres with high porosity and high specific surface area by soft template method [52]. The hard template method refers to the use of rigid templates to prepare g-C_3N_4. Silica is a common hard template for the preparation of g-C_3N_4. Yang et al. synthesized porous g-C_3N_4 spheres using spherical mesoporous porous silica foam as a hard template [53]. The template-free method does not require acid to remove the template. Liao et al. prepared g-C_3N_4 microspheres by templated solvothermal method [54]. Supramolecular self-assembly does not need templates. It can form stable structures through molecular self-assembly and non-covalent bonds. Zhou et al. created supramolecular carbon nitride using barbituric acid and melamine-cyanuric acid as monomers through electrostatic interaction or hydrogen bonding [55]. The synthesized carbon nitride has a high porosity and specific surface area. Most g-C_3N_4 are layer-stacked structures, and their performance can be improved by the decomposition of g-C_3N_4, which can be achieved by exfoliation methods. Papailias et al. exfoliated g-C_3N_4 through chemical and thermal treatment [56]. The catalytic process of g-C_3N_4 was dramatically increased by exfoliation. Because of its polymer characteristics, easy synthesis and rich chemical properties, it can be designed at the molecular level, including non-covalent functionalization, polymerization modulation, coordination interaction, hydrogen bond modulation, doping and copolymerization and covalent functionalization [57].

3. Design strategy of the atomically dispersed catalysts

Transition metal atoms have better catalytic performance and stability because of their higher single-atom utilization. The properties of single-atom dispersion can produce unsaturated coordination in the metal center, resulting in increasing surface free energy significantly [58–60]. At the same time, the quantum size effect of single metal atoms and the metal-carrier interaction make SACs have excellent performance [61]. It has been found that density functional theory (DFT) calculations show that doping of transition metals can enhance the light absorption of materials [62,63]. These have made it possible for SACs to develop well. The synthesis method has a great influence on the formation of support microstructure and active center, thus further affecting the catalytic property of the material.

SACs containing transition metals Fe, Co, Mn, Cu and Ni as active sites have been reported [62,64–66]. At the same time, it has been found that two atoms in dual-atomic site catalysts interact with each other [67]. The synthesis of ADCs is to appropriately disperse the dispersed single atom on the support. Currently, the methods for preparing single-atom catalysts using g-C_3N_4 as the support include wet chemical method, pyrolysis, atomic layer deposition (ALD) and molecular metal complexes [68]. In addition, the physical and chemical state of metal single atomic sites and the presence of single atoms can be demonstrated through a series of characterization methods, including X-ray photoelectron spectroscopy (XPS). The crystal structure was analyzed by X-ray diffraction (XRD), X-ray absorption near edge structure (XANES) and high-angle annular dark field scanning transmission electron microscope (HAADF-STEM), etc. Next, we will review the synthesis methods of SACs and DACs by combining different transition metals and corresponding preparation methods in detail.

3.1. Single-atom catalysts

Based on the introduction of g-C_3N_4 in the previous section, we will focus on synthesizing SACs anchored on g-C_3N_4. The key to preparing SACs is to make independent single atoms highly dispersed on the carrier through the interaction between the metal center and the substrate. In the current research, the standard methods for preparing SACs on g-C_3N_4 include pyrolysis, physical and chemical deposition (e.g., atomic layer deposition, chemical vapor deposition), impregnation method, hydrothermal method, ball milling, solution-phase synthesis and so on. Each method has advantages and disadvantages. At present, pyrolysis dominates the material preparation [69,70]. The preparation of one material is not limited to one way. The metal atoms can be further dispersed by proper calcination process to form isolated single atoms anchored to the carbon nitride support. More and more studies on the synthesis of SACs have adopted the strategy of multi-method joint practice. It is not appropriate to introduce the synthesis strategy of SACs according to the classification of methods. Therefore, our introduction to SACs synthesis will be expanded according to the logic of metal center classification.

Fe single-atom catalysts. Fe is cheap and has good properties in both acidic and basic solutions. Fe SACs have excellent catalytic properties in redox reactions and are the most widely studied SACs. Peng et al. prepared Fe SACs by ball milling and pyrolysis. Firstly, Fe imidazole coordination compound (Fe-ICC) as a precursor was prepared by mixing polyvinylpyrrolidone (PVP) and $FeSO_4{\cdot}7H_2O$ via ball milling. After being ground, Fe-ICC was combined with melamine as a support and carbonized for 6 h at various pyrolysis temperatures in a tube furnace with N_2 as the environment. The Fe SACs were eventually acquired. The presence of the particular electronic structure of $Fe^{\delta+}$ in the samples was demonstrated by XANES of the Fe K edge for Fe-g-C_3N_4. Fe-g-C_3N_4′s FT k^3-weighted $\chi(k)$ function EXAFS spectra showed no blatant Fe-Fe bonding. This provided additional proof of the Fe's atomic dispersion within the Fe-g-C_3N_4 catalyst. The Fe-g-C_3N_4 WT contour plots showed that isolated Fe atoms were the predominant Fe species in the catalyst as-prepared (Fig. 1 a-d) [65]. Zhou et al. synthesized Fe SACs on an oxygen-rich carbon nitride by heating a mixture of dicyandiamide (DCD), pyromellitic dianhydride (PMDA) and ferric chloride hexahydrate ($FeCl_3{\cdot}6H_2O$) at 325 °C for 4 h [71]. Huang et al. synthesized different Fe SACs catalysts by calcining the hybrid of polypyrrole (PPy) and Melamine-CA (MCA) complex containing trace Fe^{3+} ions (Fe/PPy@MCA) as C, N, and Fe resources under N_2 atmosphere [72]. By using a two-step pyrolysis process, Zhu et al. successfully synthesized the g-C_3N_4 containing single-atom FeN_5 sites [73]. ICP-AES determined that the Fe content is 16.64 wt%. A common technique for the design of Fe SACs is atomic layer deposition in addition to pyrolysis. It is a series of surface reactions that create non-noble single atoms through a self-limiting mechanism. In order to create supported Pt single atoms on N-doped carbon nanosheets for the ALD produced Fe/Pt SACs, Li et al. used g-C_3N_4 as a catalyst [74]. The outcomes of XAS show singly dispersed Fe atoms. Results from the XANES and EXAFS show that the Fe SACs achieved are in an M−pyrrolic−N_4 structure. According to the ICP-OES results, FePt NCNS has a Fe loading that is 0.6 wt% higher than Fe-NCNS, which is 1.6 wt%.

Co single-atom catalysts. Co is often used in the preparation of metal SACs. The nitrogen atoms in g-C_3N_4 are strongly bound to cobalt atoms, which can promote the kinetic and thermodynamic stability of Co SACs. Li et al. synthesized Co SACs supported g-C_3N_4 by thermal polymerization [75]. Firstly, they prepared g-C_3N_4 by annealing urea in the air. Secondly, citric acid, g-C_3N_4 and Co (II) phthalocyanine were mixed with isopropanol and acetone. Then the dried sample was heated at 655 °C and obtained the final product. The Co loading rate of the material reaches 3.17 wt%. Similarly, Wang et al. obtained Co SACs supported by g-C_3N_4 by one-pot synthesis. The cobalt salt and urea are distributed in the solution, then dried and annealed for 2 h in N_2 at 500 °C. The Co(II)-N bond in the material promotes the dispersion of the Co atom, and Co-N_4 in the material was the active site [76]. Currently, the synthesis methods of Co SACs are mainly thermal polymerization, and the heating temperature also affects the properties of materials. There are also some studies on this aspect. Li et al. mixed C_3N_5, KCl, LiCl and $CoCl_2{\cdot}6H_2O$ and heated in different temperatures (500–800 °C). On the carbon base, Co exists as a single atom. It is also found that the atomic loading rate of Co on g-C_3N_5 reaches 5.19 wt% [77]. Vitamin B12 is a kind of organic compound that contains the Co element. So, Wang

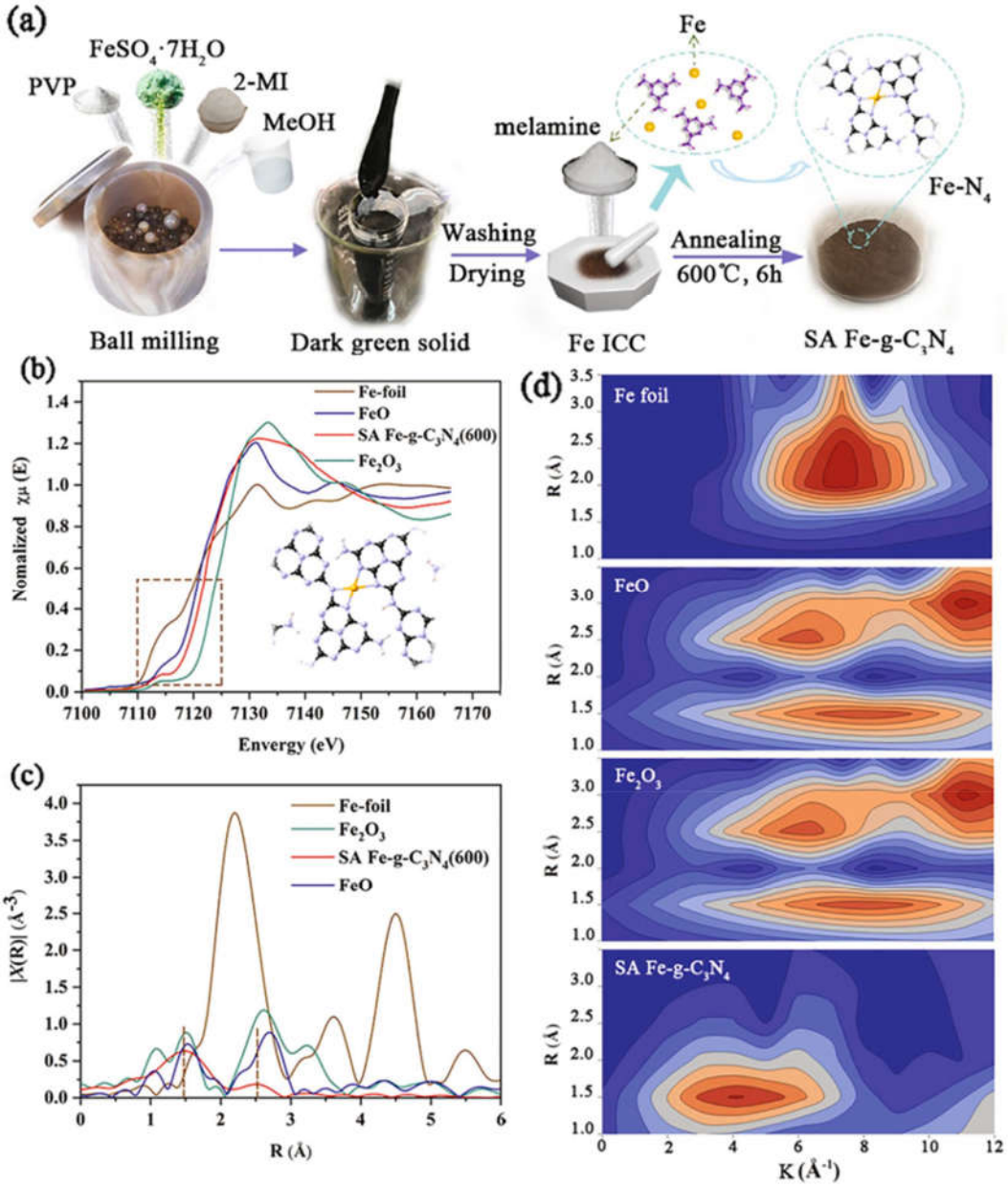

Fig. 1. (a) An example of a schematic showing how SA Fe-g-C_3N_4 catalysts are made; (b) XANES spectra at the Fe K-edge of SA Fe-g-C_3N_4 (600) and reference samples; (c) FT k3-weighted EXAFS spectra of SA Fe-g-C_3N_4 (600); (d) WT plot of SA Fe-g-C_3N_4 (600) [65].

et al. found that Co SACs could be obtained by pyrolysis of a mixture of g-C_3N_4 and Vitamin B12 [78]. The resulting solid was designated as Co-C-X, where X stood for the temperature at which pyrolysis occurred. It can be seen from the XRD analysis of Co-C-X that the structure of Co-C-X changes due to different pyrolysis temperatures. At 600 °C, there is no diffraction peak of cobalt and cobalt oxide, indicating that Co is highly dispersed on Co-C-600. Raman spectrum of Co-C-X was investigated. The proportion of carbon decreases with the increase in temperature. Nitrogen will gradually become ammonia due to temperature rise [79]. Cao et al. prepared Co SACs by wet impregnation and pyrolysis using urea, $NaH_2PO_2{\cdot}H_2O$ and $Co(NO_3)_2$ as the raw material [80]. In the preparation process, the phosphorylation of g-C_3N_4 is mainly the doping of P atoms. The exchange of P for C atoms in g-C_3N_4 is clearly shown by XPS and P solid-state nuclear magnetic resonance (NMR) studies, and the phosphorization has no impact on the structure of g-C_3N_4. Furthermore, electrochemical impedance spectroscopy (EIS) showed that P doping enhanced electrical conductivity. The Co content was about 0.3 wt%. The heavy Co atoms are primarily found as single atoms. Co SACs have an almost identical XRD pattern as g-C_3N_4 nanosheets. The brilliant spots' atomic-level resolution electron energy-loss (EEL) spectra provided additional evidence that they are Co atoms.

Cu single-atom catalysts. Cu single-atom catalysts also has attracted wide attention. Transition-metal atom Cu has the one-electron redox cycle ability [81]. Combining Cu with g-C_3N_4 results in redox sites with single-electron capacity. Xv et al. synthesized Cu-g-C_3N_4 by a simple one-pot method using melamine and $Cu(NO_3)_2$ as precursors [82]. Elemental analysis suggested that Cu was present on the g-C_3N_4 matrix in a consistent concentration. The EXAFS spectra imply that g-C_3N_4 is using the ring N sites to coordinate Cu atoms. Cometto et al. obtained Cu SACs through a method combining pyrolysis with ultrasound [83]. Firstly, they pyrolyzed melamine to produce g-C_3N_4. The final product was prepared by ultrasonic treatment of g-C_3N_4 and $Cu(NO_3)_2{\cdot}2.5H_2O$ in an argon atmosphere. The Cu loading was 14.8 wt% [84]. Liu et al. synthesized the Cu SACs by pyrolyzing coordinated polymer strategy

(PCP). They mixed formaldehyde and dicyandiamide, stirred and heated them, added $Cu(NO_3)_2{\cdot}3H_2O$ after polymerization, dried them by boiling, heated them in argon at 600°C for 2 h, and finally ground them to obtain materials. Through the ICP-OES test, the loading rate of copper atoms on Cu SACs reached 25.64 wt%. The BET surface area of Cu SACs is 60.33 m^2/g, and the print volume is 0.091 cm^3/g, both higher than g-C_3N_4. Chang et al. used surface wave plasma technology to prepare carboxyl surface defects and single-atom Cu-energized g-C_3N_4 nanosheets [85]. ICP result shows that the loading rate of a copper atom is 0.33 wt%. Attapulgite (ATP) is a kind of the one-dimensional nanomaterials with perfect performance based on its crystal structure. Liu et al. prepared Cu-ATP/PCN composite catalyst, which supported modified the Cu nanoparticles and Cu SACs [86]. Wang et al. calcined a certain amount of mixture of L-cysteine, melamine and copper nitrate in a muffle furnace to prepare a SACs co-doped with Cu and S [87]. It is also discovered that the addition of Cu and S can lengthen the distance between p-CN matrix planes, which enhances the BET and pore size of Cu SAs/p-CNS. By using ICP-OES, it was discovered that the Cu loading concentration of Cu SAs/p-CNS was 1.41 wt%.

Ni single-atom catalysts. Ni is abundant in elements and has a high electron density on Earth. It is frequently utilized to create single-atom materials. Liu et al. prepared Ni-SA by adding Phytic acid (PA) adhesive. The atomic loading rate of this material is from 0.07 to 5.68 wt% [88]. During the preparation process, the proper addition of some adhesives can increase the atomic loading rate. By thermally polymerizing urea/thiourea complexes of nickel and calcining them with NH_4Cl thereafter, Xv et al. created a single-atom Ni/S co-doped g-C_3N_4 (Ni/S-CN-N) [66]. The specific surface area of Ni/S-CN-N as measured by N_2 adsorption–desorption isothermal is 104.0 m^2/g higher than those of g-C_3N_4-NH_4Cl-assisted secondary calcination results in an increase in specific surface area. Results from FT and WT-EXAFS show that Ni/S-CN contains atomically-dispersed Ni. Similarly, Hou et al. obtained Ni/S-CN by

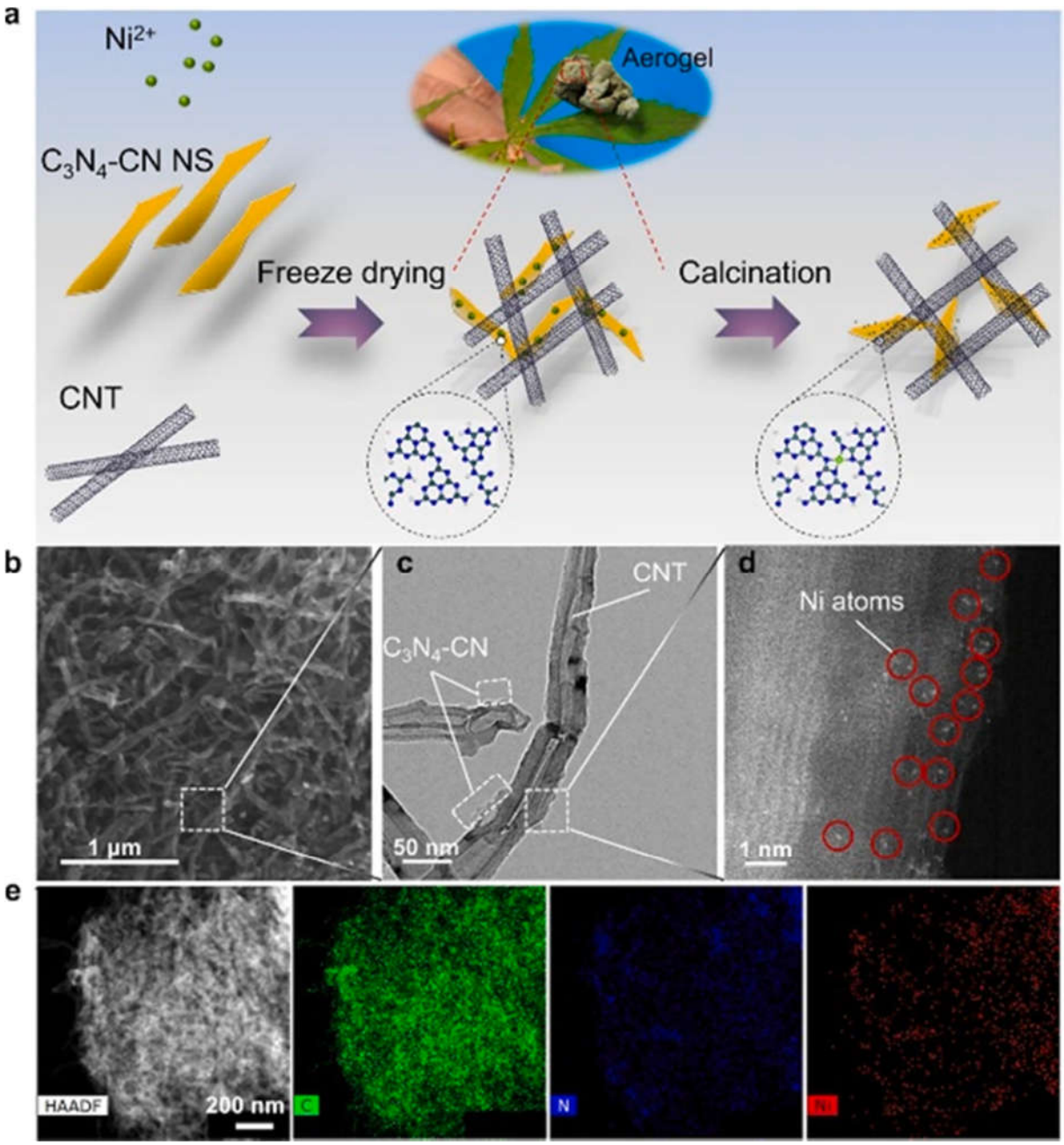

Fig. 2. (a) Schematic illustration of the preparation; (b) SEM image; (c) HRTEM image; (d) HAADF-STEM image; (e) EDS mapping image [90].

hydrothermal method [89]. The Brunauer-Emmett-Teller (BET) surface area is 235 m^2/g, and the Ni content of Ni-CN is 0.2 wt%. In addition, wang et al. composed Ni-SACs [90]. They firstly prepared g-C_3N_4 nanosheets via exfoliation methods, then the g-C_3N_4 and $NiCl_2$ aerogels were heated to 600 °C at a rate of 5 °C/min in an environment of argon. The Ni content in Ni SACs was estimated to be 1.17 wt% by ICP-OES. The single-atom character of the Ni sites for Ni SACs was confirmed by the SEM, HRTEM, and HAADF-STEM data (Fig. 2 a-e). Hai et al. obtained Ni SACs with high metal loading rates by a combination of impregnation and two-step annealing [91]. Firstly, metallic precursors were prepared by impregnation of $NiCl_2{\cdot}6H_2O$ and polymeric carbon nitride (PCN). The removal of ligands can be regulated by setting the annealing temperature below the decomposition temperature of the metal precursor. Secondly, the use of metal chloride provides better control. The chemisorbed metal precursor is then removed by a second step of annealing at higher temperatures (550 °C). Finally, the Ni SACs was obtained. To comprehend the molecular level of the synthesis mechanism, DFT calculations were performed.

Mn single-atom catalysts. Mn-based materials have high catalytic activity and low toxicity. Mn SACs have attracted great interest. Mn acetate, CNTs, and dicyandiamide are thermally pyrolyzed at 600℃ in the presence of nitrogen, then they are washed with hydrochloric acid, Feng et al. created Mn-C_3N_4/CNT. The addition of CNTs improved the conductivity of g-C_3N_4 [26]. The BET of Mn-C_3N_4/CNT is 221 cm^2/g. The structural characteristics of Mn-C_3N_4/CNT were investigated using quantitative EXAFS curve fitting analysis. The single atom Mn is thrice coordinated by N atoms due to the Mn-N coordination number of 3.2. The presence of atomically scattered Mn in Mn-C_3N_4/CNT is confirmed

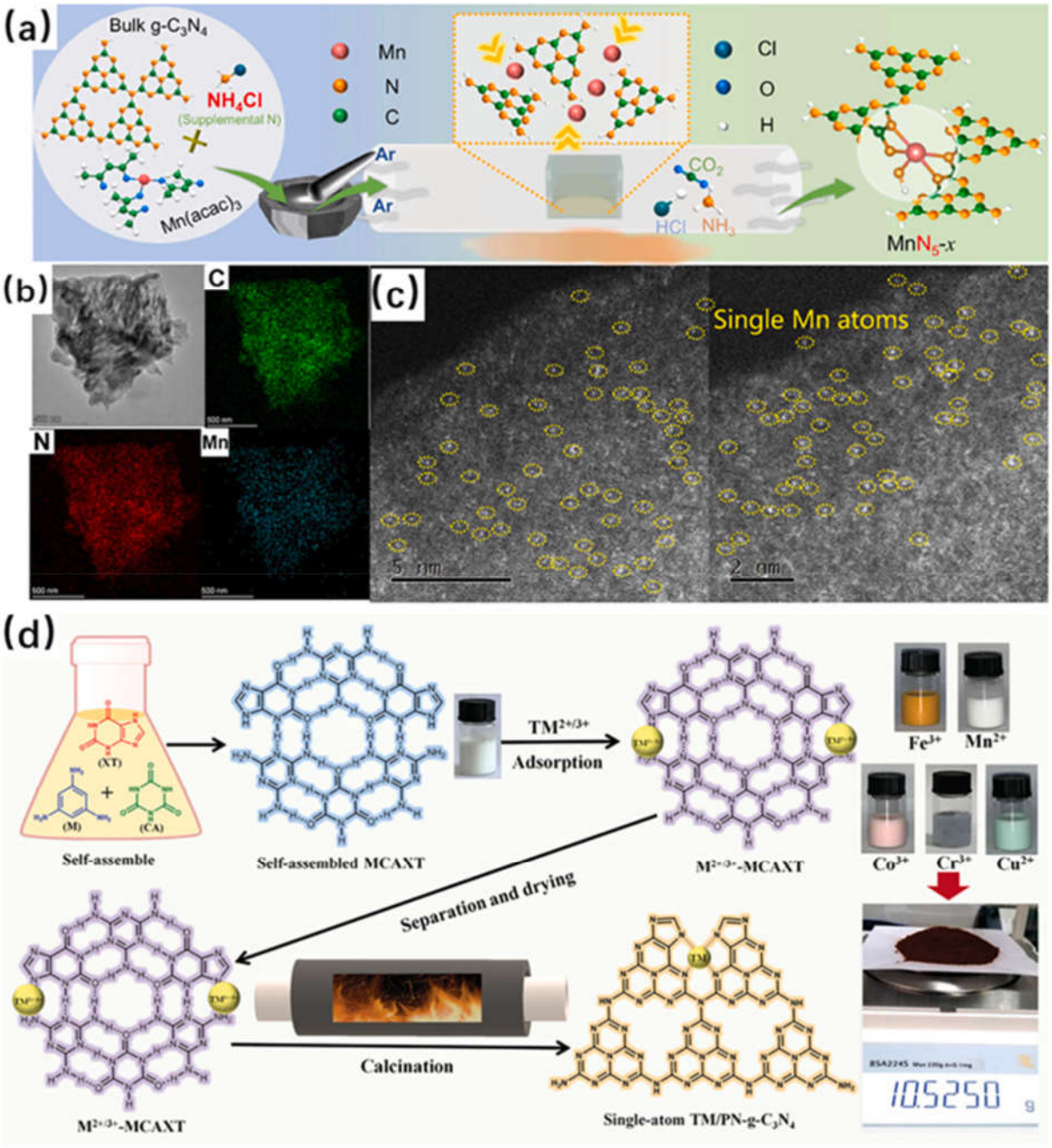

Fig. 3. (a) Schematic procedure for the synthesis of Mn SACs; (b) EDS-mapping images; (c) HAADF-STEM images of Mn SACs [93]; (d) Schematic illustration of the large-scale production of the SA-TM/PN-g-C_3N_4 [95].

by the HAADF-STEM picture, and the Mn content was found to be 0.17 wt% as determined by ICP-OES. Yang et al. obtained Mn SACs with a coordination structure of Mn-N_4 by hydrothermal method [92]. A stronger peak may be seen at about 1.3 in the Mn-CN Fourier-transformed (FT) extended X-ray absorption fine structure (FT-EXAFS) spectrum. This points to the existence of a solitary Mn atom. SACs with coordination numbers higher than four have rarely been reported. Due to the creation of precursors with four-nitrogen coordinated structures, direct calcination with carbon nitride and transition metal sources typically produces M−N_4. Miao et al. added external nitrogen sources (NH_4Cl) to increase the amount of nitrogen coordination during Mn-CN synthesis·NH_3 generated above 500 °C can enable amino groups to anchor on metal sites to form additional coordination structures (Fig. 3 a-c) [93]. Finally, the Mn-N_5 coordination structure was formed. The atomic loading rate of the manganese single-atom material ranges from 2.7 to 3.0 wt%. Wang et al. synthesized the MCN through $Mn(acac)_2$ and urea in-situ thermal polymerization [94]. Based on ICP-AES, the mass loads of Mn after nitration in Mn-SACs is 3.06 wt%. In addition, a variety of g-C_3N_4 based transition metal single atom have been prepared through the combination of self-assembly and calcination of various precursors (Fig. 3 d).

3.2. Dual-atom catalysts

The M−N−C active center formed by binding transition metal atoms with g-C_3N_4 plays an essential role in the transition metal's catalytic activity by regulating the transition metal's d-band center. Moreover, the chemical bonds between transition metal atoms and doped nonmetal atoms also enhance the catalytic activity. It has been shown that single atoms of bi-transition metals can improve bandgap modulation through the strong interaction between metals and the synergistic effect [96]. In addition, Some studies have shown that DACs are more effective than single-atom catalysts in removing metal nuclei, forming a good activated porous graphite carbon layer [97]. In recent years, new atomically dispersed catalysts have emerged [98,99]. Moreover, some studies have shown that the introduction of a second metal center into the first metal center in the catalyst can promote activation [100], and in addition, the scaling relationship is likely to be destroyed during synthesis or catalysis [101]. The preparation methods of diatomic catalysts mainly include atomic layer deposition (ALD) [102], impregnation-adsorption [103], and high-temperature pyrolysis strategies [104]. Pyrolysis of a variety of metal precursors premixed with the bulk material is a common method to introduce a polymetallic center on a single support. ALD and impregnation-adsorption methods can provide high-quality DACs.

Yao et al. synthesized externally dispersed NiCu DACs on nitrogen-doped graphene by pyrolysis of a mixture of dicyandiamide, glucose, nickel, and copper salts in an argon atmosphere [106]. TEM images showed that the obtained NiCu-CN samples had multilayer thickness corrugated nanosheets. Moreover, the defect layer morphology is conducive to the uniform anchoring and dispersion of metal atoms. XRD analysis and TEM images of the obtained samples showed no significant aggregation, indicating the formation of solitary Ni and Cu sites. Utilizing bulk g-C_3N_4 and glucose as the support and stabilizers, respectively, Wan et al. produced NiFe-g-C_3N_4 utilizing a straightforward molecule-based tailoring technique [107]. The use of glucose can fix single metal atoms and prevent metal atoms from aggregating. Glucose acts as a catalyst during high temperature pyrolysis to further convert glucose chelated g-C_3N_4 attached to metal atoms into N-doped graphene. The metal composition of the SACs is 7.5 wt% for NiFe-CN. In addition, L-alanine (amino acid), ferric (II) acetate, nickel (II) acetate tetrahydrate, and melamine were used by Zeng et al. to create a NiFe-DASC catalyst via ball milling and pyrolysis [105]. The creation of single or double layers of graphene is indicated by the presence of porous carbon nanosheets in TEM and SEM. The nitrogen-doped graphene support contained both Ni and Fe atoms, as shown by dark-field scanning TEM and energy dispersive X-ray spectroscopy (EDS) of NiFe-DASC. Further demonstrating the existence of discretely distributed Ni and Fe atoms is HAADF-STEM. The pair of atoms' typical distance was also found to be 0.24 nm, which raises the possibility of a metal–metal contact. The EELS provided additional evidence that the bright spots were Ni and Fe atoms (Fig. 4 a-g).

By using dicyandiamide as a carbon source, iron phthalocyanine (FePc) and manganese nitrate ($Mn(NO_3)_2$) as metal precursors, Yang et al. prepared bimetallic atom-dispersed Fe and Mn/N-C electrocatalysts through thermal polymerization and pyrolysis, and successfully implanted Mn-N part into the traditional Fe/N-C system (Fig. 5 a-d) [108]. The many atomically scattered metal-nitrogen in Fe, Mn/N-C are linked to the Fe/Mn-Nx bond, which has a binding energy of 399.1 eV. These combined HAADF-STEM, EDS elemental mapping, EELS, and metal pair distance measurements attest to the coexistence of Fe and Mn as Fe/Mn atomic pairs. With many micropores and mesopores, Fe, Mn/N-C has a specific surface area and pore volume of 245.33 m^2/g and 0.3 m^3/g, respectively.

Zhou et al. designed FeNi DACs coordinated with N and P in porous g-C_3N_4 via defect strategy and soft templates method. Firstly, they produced porous g-C_3N_4 from melamine, cyanuric acid and uramil by thermal polymerization. Secondly, they used $Fe(NO_3)_3·9H_2O$, $NiSO_4·6H_2O$, urea to form mixture. And then, the mixture was placed in a Teflon-lined autoclave, and FeNi-LDH powders were collected. In order to produce CN-FeNi-P, the mixture was calcined for a final time for 2 h at 350 °C in a N_2 atmosphere while utilizing NaH_2PO_2 as a PH_3 atmosphere [109]. ICP testing reveals that the loading amounts of Fe and Ni are 0.36 and 1.01 wt%, respectively. Single atoms can increase the specific surface area of a porous arrangement like this and enhance mass transfer. In this material, the two metals are connected by a P bridge. The coordination information of two metal atoms was investigated by XANES, EXAFS, and wavelet transform (WT), demonstrating that the Fe atoms are scattered as solitary particles. Results from EXAFS and WT demonstrate that Ni is in conjunction with N and P and has an atomical distribution. Similarly, Yu et al. design and synthesize P-induced Fe and Co single atoms by an external PH_3 annealing treatment using soft-template precursors [110]. In electrical structure modulation, P is crucial. In addition, oxygen-doped g-C_3N_4. In order to accelerate the breakdown of organic contaminants, O-g-C_3N_4 may be used [111]. Wang et al. prepared Fe-Co-O-g-C_3N_4 co-doped with the dual-atomic site and nonmetallic through calcination [112].Co/Mo-MCN was prepared through MoS_2 ethanol solution, guanidine hydrochloride and $CoCl_2·6H_2O$ according to the same calcination process described above. A similar mesoporous structure with a high specific surface area can increase the charge carrier separation efficiency, thereby improving the catalytic activity [113]. Wang et al. synthesized the porous few-layer g-C_3N_4-Co_xNi_y [114]. First, the self-assembly of melamine and its hydrolysate was controlled to create microtubular precursors using protonated phosphoric acid. To exfoliate g-C_3N_4, ethanol and glycerol were introduced as an inserter. The cavity of the g-C_3N_4 was then filled with sources of Ni and Co. Finally, the thermal polycondensation process would result in the production of porous few-layer g-C_3N_4-Co_xNi_y from the liberated gas. In addition, Zhao et al. used ferric chloride, cobalt chloride and formamide to produce FeCo-N/C by hydrothermal method and pyrolysis [115]. The contents of Co and Fe of FeCo-N/C were determined by ICP-MS to be 2.01 and 3.32 wt%, respectively. The BET of FeCo-N/C was calculated to be 68.4 m^2/g. The high level of active site availability and effective electron transport at the catalyst/reactant contact are indicated by this.

Other metals were also used to prepare dual-atomic site materials in addition to the transition metal. The embedding of noble metals into transition metal single-atomic materials can realize the expansion of noble metal geometry and obtain tunable interatomic interactions. At the same time, the catalyst will have metal–metal interaction and metal-support interaction [116]. Cheng et al. found that the synergy between Co and Ru and the combination of atom-specific features can greatly

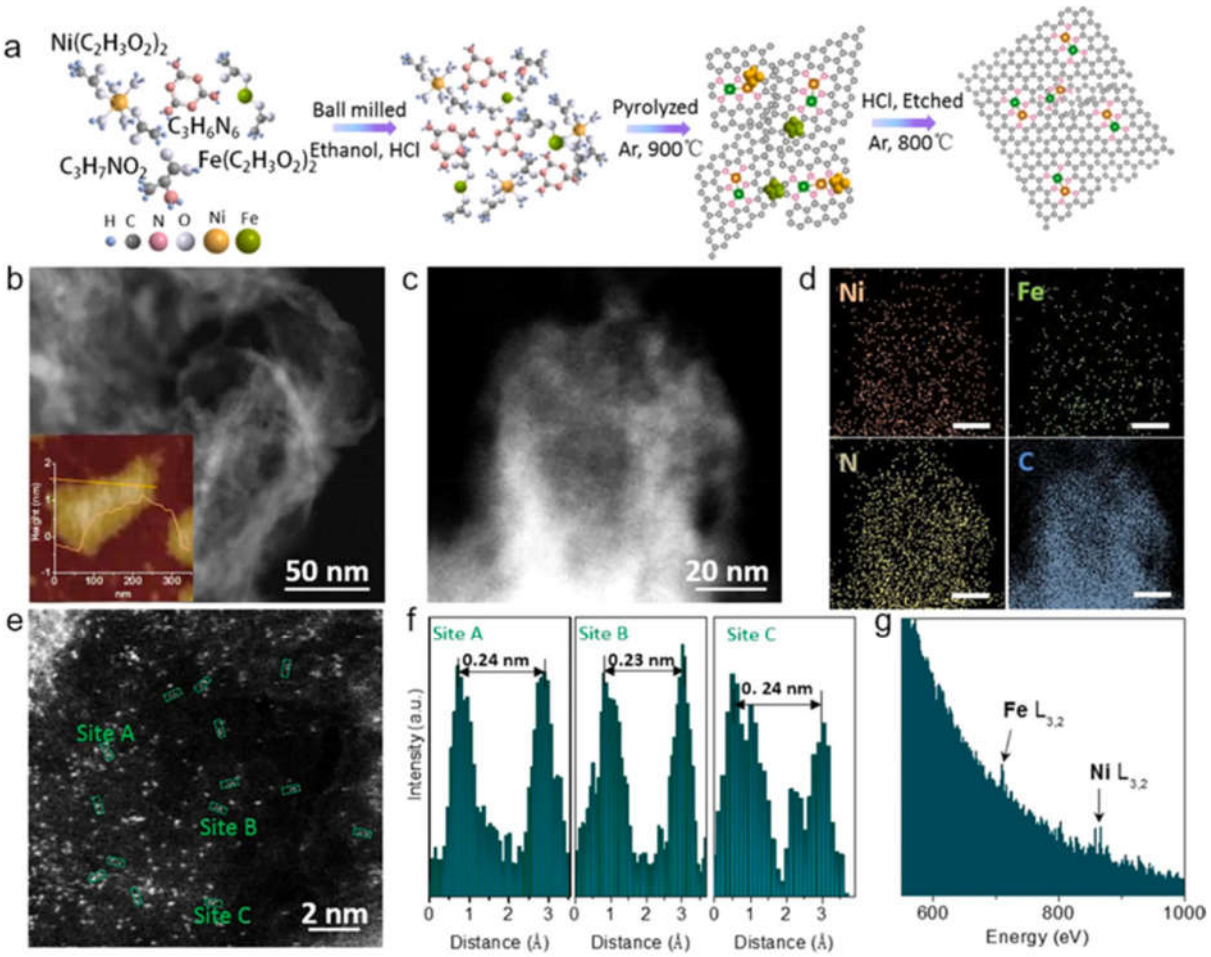

Fig. 4. (a) Schematic illustration of NiFe-DASC synthesis; (b) Dark-field scanning TEM and AFM (inset) images; (c) TEM image and (d) EDS elemental mapping of NiFe-DASC; (e) HAADF-STEM image of NiFe-DASC with some diatomic pairs being highlighted by green rectangles; (f) Intensity profiles of the three sites in (e); (g) EELS of NiFe-DASC [105].

promote photocatalytic performance. Through a simple self-seeded procedure involving formamide condensation and carbonization, they were able to insert the atomic Co-Ru bimetal into a conjugated carbon nitride polymer [117].

The preparation processes for the aforementioned g-C_3N_4 based ADCs are summarized in Table 1. Through the above analysis, it is found that iron, cobalt and copper SACs can achieve high metal loading rates, while manganese and nickel SACs have low metal loading rates. Most DACs adopt the pyrolysis method and ALD method, and most DACs adopt the combined strategy of both. Firstly, the anchoring of single metal atoms is carried out, and then the second metal is fixed in the g-C_3N_4 matrix by the chemical deposition method or pyrolysis method. Through the introduction of different transition metal SACs designs, we find that different synthesis methods have been developed. The design strategies of SACs include pyrolysis, wet impregnation, physicochemical deposition, ball milling and so on. The wet impregnation method is simple and easy, and the metal load rate is low. Physical and chemical deposition methods can better control metal sites. The ball milling method is simple in application and more used in the treatment of precursor, and the method can increase the specific surface area of the catalyst. Pyrolysis is the most common method for preparing atomically dispersed metal sites. During the pyrolysis process, transition metal atoms can easily coordinate with heteroatoms in the g-C_3N_4 matrix. By simply controlling the composition and temperature of the low-cost precursor, the high metal load level and the coordination structure can be controlled. In AOPs, additional attention should be paid to the problem of metal loading, and the optimal amount of single atoms should be introduced while ensuring the stability of the g-C_3N_4 skeleton to prevent structural damage and metal leaching. In addition, the preparation of single atoms by wet chemical method requires pretreatment of the precursor material to reduce unwanted ligands and prevent the aggregation of metal atoms. However, too many metal atoms will cause agglomeration. In particular, the impregnation method and co-precipitation method should pay great attention to the amount of metal added. Therefore, to ensure the stability of g-C_3N_4 matrix and high utilization rate of single atoms, it is essential to control the loading of metal atoms and develop efficient strategies to anchor metal atoms to achieve isolated dispersion. In addition, the existence and spatial configuration of single atoms can be confirmed by some characterization methods. Individual metal atoms can be observed with a scanning tunneling microscope (STM) [118]. X-ray absorption Near Edge spectroscopy (XANES) and Extended X-ray Absorption Fine Structure (EXAFS) spectroscopy techniques can identify clusters with dispersed single atoms [119], as well as other species information. Infrared (IR) spectroscopy can quantitatively confirm the presence of individual metal atoms [120].For the application and advancement of SACs in the realm of environmental remediation, improving the synthesis and quality of SACs by optimizing the synthesis process is crucial.

4. Applications in the environment

As heterogeneous catalysts, g-C_3N_4-based ADCs have received a lot

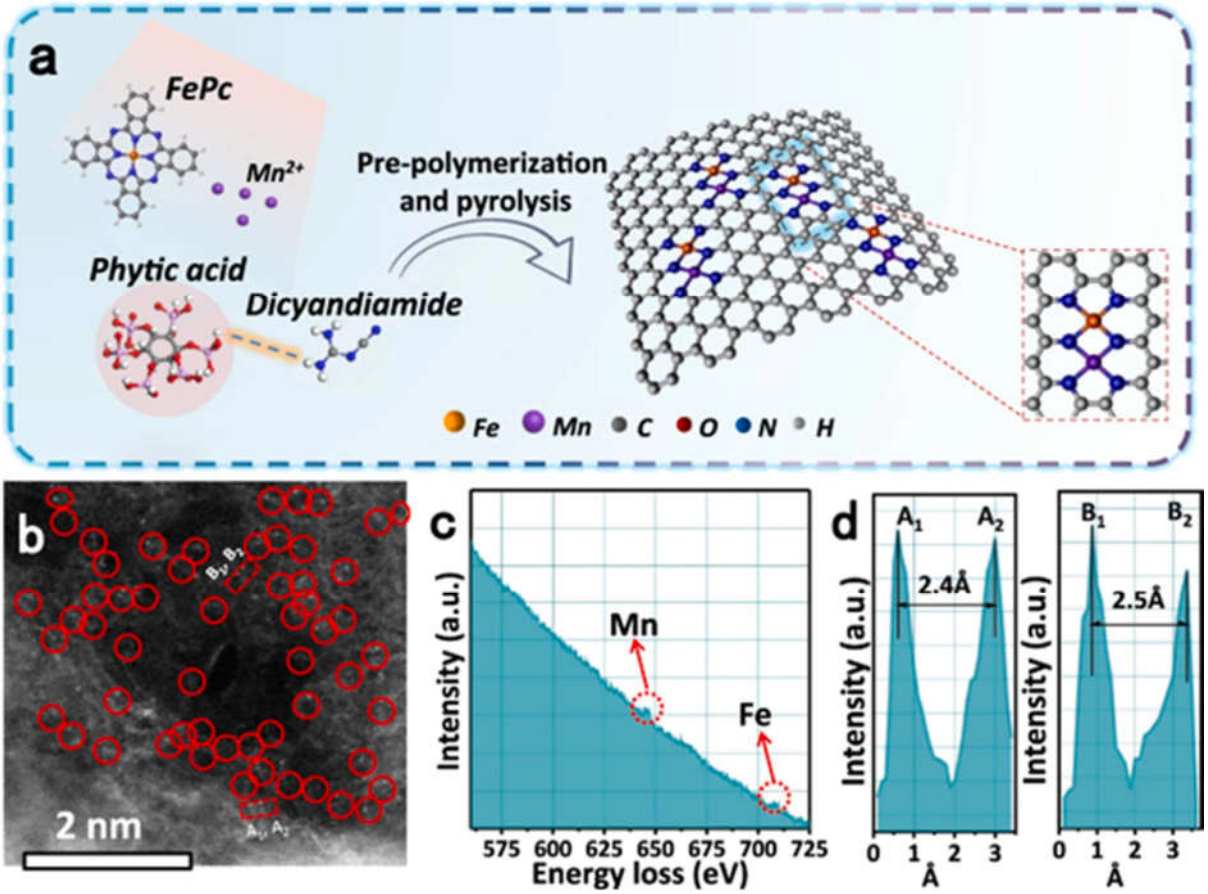

Fig. 5. (a) Synthetic image and TEM characterizations of Fe, Mn/N-C catalyst; (b) HAADF-STEM image of Mn, Fe/N-C with mappings of individual elements (C, N, Fe, and Mn); (c) Fe, Mn/N-C structure analyzed by EELS; (d) The intensity profiles were obtained on two bimetallic Fe–Mn sites [108].

Table 1
Summary of the various g-C_3N_4-based ADCs for preparation methods.

Metal atom	g-C_3N_4-based ADC	Synthetic raw material	Synthesis methods	Metal loading (wt%)	BET surface (m^2 g^{-1})	Reference
Fe	SA Fe-g-C_3N_4	PVP, 2-MI, MeOH, $FeSO_4·7H_2O$	Ball milling, Pyrolysis	4.07	50.8655	[65]
	Fe-N-C/CN 800	Ppy, MC, $FeCl_3·6H_2O$	Calcining	11	127.5	[72]
	Fe-NPs/NCNS	Ferrocene, Urea	ALD	0.6	–	[74]
Co	SACo@g-C_3N_4	$C_6H_8O_7$, CoPc	Pyrolysis	3.17	211	[75]
	Co-C-SACs-700	Vitamin B12, Urea	Pyrolysis	4.35	60.1	[79]
	Co/PCN.	Urea, $NaH_2PO_2·H_2O$, $Co(NO_3)_2$	Thermal polymerization, wet impregnation	0.3	–	[80]
Cu	Cu SACs	Melamine, $Cu(NO_3)_2·2.5H_2O$	Pyrolysis, Ultrasound	14.8	–	[84]
	Cu SACs	Dicyandiamide, $Cu(NO_3)_2·3H_2O$	Pyrolysis	25.64	60.33	[62]
	Cu SAs/p-CNS	Melamine, L-cysteine, Cu nitrate	Calcining	1.4	13.6901	[87]
Ni	Ni-SA/CN	Urea, $Ni(Ac)_2·4H_2O$, PA	Pyrolysis	5.68	–	[88]
	Ni/S-CN-N	Urea, Thiourea, $Ni(NO_3)_2·6H_2O$	Thermal polymerization	3.39	104.0	[66]
	Ni/S-CN	Dicyandiamide, Thiophene, $NiCl_2$	Hydrothermal method	0.2	235	[89]
	Ni SACs	Dicyandiamide, $NiCl_2·6H_2O$	Impregnation, Annealing	10	–	[91]
Mn	Mn-C_3N_4/CNT	Mn acetate, CNTs, Dicyandiamide	Pyrolysis	0.17	221	[26]
	MnISAs@CN	$Mn(acac)_3$, 2-Methylimidazole	Hydrothermal method	0.27	1159.2	[92]
	Mn SACs	Dicyandiamide, NH_4Cl, $Mn(acac)_3$	Calcination	2.7–3.0	–	[121]
	MCN	Urea, $Mn(acac)_2$	Thermal polymerization	3.06	–	[94]
DACs	NiCu DACs	$NiCl_2·6H_2O$, $CuCl_2·2H_2O$, Dicyandiamide, Glucose	Pyrolysis	0.67; 0.88	–	[106]
	NiFe-DASC	Melamine, L-alanine, Fe(II) acetate/Ni(II) acetate	Ball milling, pyrolysis	4.05; 3.2	433.2	[105]
	Fe, Mn/N-C	Dicyandiamide, FePc, $Mn(NO_3)_2$	Pre-polymerization, pyrolysis	2.3; 1.6	245.33	[108]
	CN-FeNi-P	Melamine, Cyanuric acid, Uramil, $Fe(NO_3)_3·9H_2O$, $NiSO_4·6H_2O$, Urea	Hydrothermal, Pyrolysis	0.36; 1.01	–	[109]
	Fe-Co-O-g-C_3N_4	Urea, oxalic acid, $FeCl_3·6H_2O$, $CoCl_2·6H_2O$	Pyrolysis	2.3; 2.6	20.24	[111]
	g-C_3N_4-$Co_{1.6}Ni_{0.4}$	Melamine, PA, $Ni(NO_3)_2·6H_2O$, $Co(NO_3)_2·6H_2O$	Calcination	1.27; 0.84	153.17	[114]
	FeCo-N/C	$FeCl_3$, $CoCl_2$, Formamide	Hydrothermal, Pyrolysis	3.32; 2.01	68.4	[115]

of attention recently. Unique characteristics of g-C_3N_4 include its rich functional groups, moderate energy gap, exceptional electrical properties, and surface imperfections. In addition, SACs have maximum atomic utilization, particular electronic structure and favorable coordination structure. These materials are essential in AOPs for removing organic pollutants, including photocatalysis and Fenton-like reactions (H_2O_2, PMS, and PDS). The figure summarizes several applications of ADCs (Fig. 6). The carbon substrate can adjust the catalytic site of the material. Each system produces active species and, through different oxidation pathways to remove contaminants. The interaction of single atoms with the matrix gives the composites unique physicochemical properties that also play a significant role in the field of electrocatalysis [122], including technologies such as fuel cells, oxidation–reduction reactions (ORR) and environmental remediation. Transition metal atoms can be firmly combined with nitrogen atoms on g-C_3N_4, thus the spill of metal elements can be inhibited and the toxicity of catalyst can be effectively avoided. At the same time, metal atom doping can effectively change the electronic structure of the carbon base, thus effectively activating PMS [123]. It has also been found that the carbon nitride based single-atom material has good catalytic activity for pollutants under visible light irradiation [25]. Table 2 summarizes some of the ADCs mentioned in this paper for the degradation of pollutants in AOPs.

4.1. Photocatalysis

Carbon nitride has proved to be an excellent photocatalytic material because of its nontoxicity, easy synthesis, and high stability. It has been found that single-atom modification of g-C_3N_4 can significantly improve the efficiency of photogenerated carrier separation, especially transition metal atoms, which is beneficial to the photocatalytic reaction. In recent years, a novel technique to increase the photocatalytic activity of semiconductors has been developed: homogeneous dispersion of single-atomic metal sites into carbon matrix through coordination bonds [124]. Single-atom materials can effectively enhance optical absorption, raising electron density, and encouraging charge transfer [25,53,125]. In addition, DACs have excellent performances in photocatalysis, such as band structure modulation of light absorption, active site engineering of adsorption and desorption, and charge migration mechanism.

Photo-Fenton degradation is an excellent way to treat antibiotics. Recent studies have built and used heterojunctions of g-C_3N_4 and single atom Co supported on N-rich carbons as heterogeneous catalysts for PMS activation. Qian et al. have successfully prepared the heterojunctions of Co SACs and g-C_3N_4 [126]. As shown in Fig. 7 a-e, the heterojunction structure of Co SACs with g-C_3N_4 can regulate charge transfer and promote the redox reaction at the Co site. Electron transfer across heterojunctions leads to enhanced degradation efficiency of photo-fenton reaction. From the comparison of ROS concentrations in different systems, it is obvious that the synergistic effect of the two promoted the increase of ROS production. The research showed that SA-Co-CN/g-C_3N_4/PMS system could effectively degrade and oxidize various antibiotics. The synergistic interaction of the photoactive g-C_3N_4 substrates with the island-like Co-CN SACs increases ROS generation. Active substances that play a role in the system include •OH, $^1O_2$ and $O_2^{\bullet-}$. The hydroxyl group plays a major role. The SA-Co-CN/g-C_3N_4 heterojunction is made more conducive to electron transfer by the combined action of visible light and Co SACs, which in turn speeds up the redox cycle of Co^{2+}/Co^{3+} for PMS activation.

$$Co^{2+} + HSO_5^- \rightarrow Co^{3+} + SO_4^{\cdot-} + OH^- \quad (1)$$

$$Co^{2+} + HSO_5^- \rightarrow Co^{3+} + SO_4^{2-} + \cdot OH + H^+ \quad (2)$$

$$SO_4^{\cdot-} + H_2O \rightarrow SO_4^{2-} + \cdot OH + H^+ \quad (3)$$

$$Co^{3+} + e^- \rightarrow Co^{2+} \quad (4)$$

$$Co^{3+} + HSO_5^- \rightarrow Co^{2+} + SO_5^{\cdot-} + H^+ \quad (5)$$

$$2SO_5^{\cdot-} \rightarrow 2SO_4^{2-} + 1O_2 \quad (6)$$

Dong et al. proved that limiting atomic dispersed Cu to g-C_3N_4 (Cu-C_3N_4) can rapidly activate H_2O_2 and effectively separate photogenerated electron-hole pairs, hence enhancing the degradation efficiency of the photo-Fenton reaction [127]. The photo-degradation rate of ciprofloxacin (CIP) is close to 99 % in 30 min. Additionally, it was

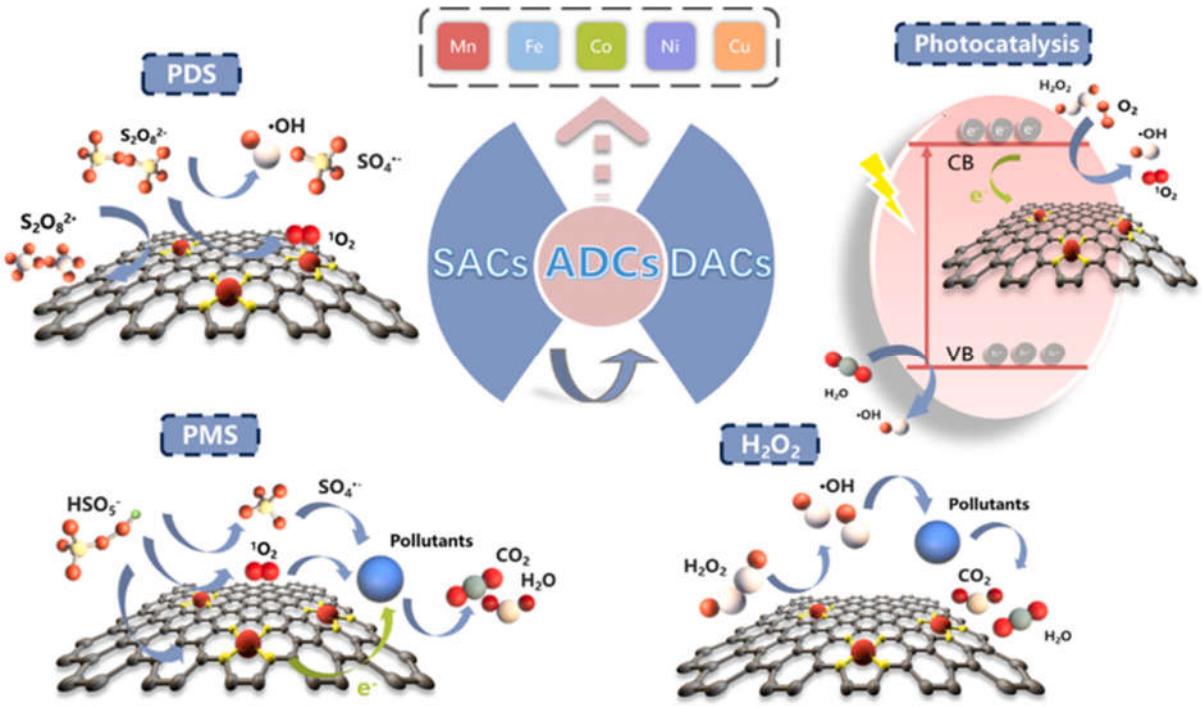

Fig. 6. Application of ADCs in AOPs such as H_2O_2 activation, PMS activation, PDS activation, and photocatalysis.

Table 2
Summary of the various g-C_3N_4-based ADCs for AOP applications.

Catalysts	AOP application	Pollutants	Removal efficiency	Pseudo-first-order rate (min^{-1})	Stability (Removal efficiency after recycling)	Reference
Ni-SACs/g-C_3N_4	Photo	BPA	94.1 % in 60 min	0.0157	–	[88]
Mn-CN-2	Photo	TC	82 % in 40 min	0.041	5 cycles, 82 %	[94]
P-Fe_1Co_1/CN	Photo	TBBPA	96 % in 120 min	–	–	[110]
Fe-g-C_3N_4	PMS/Photo	SMX	98.7 % in 6 min	0.602	5 cycles, 92 %	[132]
SA-Co-CN	PMS/Photo	SMX	100 % in 30 min	0.2601	10 cycles, 90 %	[126]
Cu-C_3N_4	H_2O_2/photo	CIP	99 % in 30 min	0.0978	5 cycles, 100 %	[127]
Fe_1-Nv/CN	H_2O_2/Photo	CIP	91 % in 60 min	0.04837	–	[130]
I-FeNx/g-C_3N_4	H_2O_2/Photo	MB	98.9 % in 11 min	0.56	4 cycles, 98 %	[160]
SAS-Cu	PS/Photo	TC	82.5 % in 30 min	0.0679	4 cycles, 67.9 %	[62]
Cu-C_3N_4	H_2O_2	RhB	97.5 % in 5 min	–	5 cycles, 100 %	[82]
$Fe_{0.4}Cu_{0.6}$-N-C	PDS	TBBPS	98.7 % in 5 min	0.06	5 cycles, 78.7 %	[144]
SA-CoCN	PMS	BPA	100 % in 40 min	0.073	5 cycles, 80 %	[76]
SA Fe–g–C_3N_4(600)	PMS	TC	93.29 % in 40 min	0.045	4 cycles, 81 %	[65]
Mn SACs	PMS	4-CP	100 % in 6 min	0.0518	6 cycles, 99 %	[121]
Fe/CN	PMS	4-CP	–	0.55	–	[135]
SA-Cu/rGO	PMS	SMX	99.6 % in 60 min	–	5 cycles, 91.6 %	[84]
Co-SACs	PMS	CIP	99.8 % in 20 min	0.287	5 cycles, 95.2 %	[139]
Fe/Co-N-C	PMS	Phenol	100 % in 31 min	0.417	5 cycles, 92 %	[115]

discovered that a non-free radical reaction pathway was responsible for the photo-Fenton catalytic performance, in which the formation of O = Cu-N_4 = O intermediate activated H_2O_2. Liu et al. discovered that the band gap was decreased and the separation of photo-generated carriers was further encouraged by the doping of a single atom of Cu. [86]. The pace of MB degradation has significantly increased, and it can now be attributed to the interaction of the superoxide radical (•O_2^-), the hydroxyl radical (•OH), the electron (e^-), and the hole (h^+). Liu et al. synthesized Ni-SACs/g-C_3N_4 catalyst and applied it to BPA degradation. The degradation of BPA by Ni-SACs/g-C_3N_4 reached 94.1 % in 60 min. The results of the trapping tests show that the main active species in the photooxidation of BPA are •O_2^- and photoexcited holes. Two active photocatalytic sites, Ni-N_4 and g-C_3N_4, each play a unique function in the process. It is revealed that Ni-N_4 sites with low loading enable quick dynamics of charge carriers to separate and transfer, allowing for the accumulation of additional hot electrons. Due to the nearby Ni single-atom's confined metallic character in the carbon nitride matrix, the single-atom at high loading has a suppressing impact on the production of active hot carriers.

In recent years, SACs have been used to study the photocatalytic treatment of organic pollutants. Liu et al. present a novel strategy to efficiently breakdown organic pollutants utilizing persulfate in conjunction with single-atom catalysts' high efficiency and LED light sources' low energy consumption. The experimental data showed that in the presence of persulfate (PS) and catalyst, the degradation rate of tetracycline (TC) was 82.5 % in 30 min of LED irradiation. The utilization rate of oxidizer was significantly enhanced. SAC-$Cu_{1.0}$ can be stimulated by UV light to create e^-, h^+, and the associated free radicals (•OH, •O_2^-), as well as $^1O_2$. PS is also triggered at the same time to create SO_4•$^-$. PS may also function as an electron acceptor to improve the effectiveness of electron transfer. The interaction of SO_4•$^-$, •OH and •O_2^- enhanced the formation of $^1O_2$. Finally, the efficient and quick breakdown of TC in this system is realized by the synergistic interaction of UV-light, SAS-$Cu_{1.0}$, and PS.

$$SAS-Cu_{1.0} + hv \rightarrow SAS-Cu_{1.0}(h^+ + e^-) \quad (7)$$

$$S_2O_8^{2-} + e^- \rightarrow SO_4^{\cdot-} + SO_4^{2-} \quad (8)$$

$$S_2O_8^{2-} + hv \rightarrow 2SO_4^{2-} \quad (9)$$

$$e^- + O_2 \rightarrow \cdot O_2^- \quad (10)$$

$$\cdot O_2^- + h^+ \rightarrow {}^1O_2 \quad (11)$$

$$2\cdot O_2^- + 2H_2O \rightarrow H_2O_2 + 2OH^- + {}^1O_2 \quad (12)$$

$$2SO_4^{\cdot-} + H_2O \rightarrow 2SO_4^{2-} + \cdot OH + H^+ \quad (13)$$

$$\cdot O_2^- + e^- + 2H^+ \rightarrow H_2O_2 \quad (14)$$

$$H_2O_2 + e^- \rightarrow \cdot OH + OH^- \quad (15)$$

$$\left(h^+, \cdot O_2^-, {}^1O_2, SO_4^{\cdot-}, \cdot OH\right) + TC \rightarrow intermediates \rightarrow CO_2 + H_2O \quad (16)$$

Cu single-atom material can strengthen the interlayer connections, optimize the electronic structure, and improve optical absorption and carrier transfer efficiency [128]. By introducing double sites of Cu and S, the Cu atomic site captured photoacoustic electrons, and the S atomic site had photogenerated holes, Wang et al. promoted the separation of photogenerated charge carriers and improved the conversion rate of 5-hydroxymethyl furfural (HMF) into 2, 5-dimethylfuran (DFF), showing high photocatalytic activity [87]. In addition, Lu et al. prepared Fe-Cu DACs, and a large number of Cu-Fe QDS generated more active sites, which enhanced TC adsorption and accelerated charge separation and transfer. The multiple effects of adsorption-catalytic degradation and photocatalysis-Fenton oxidation were promoted [129]. At the same time, it has been found that the introduction of single atom Mn through Mn-N/O coordination can reduce the band gap and encourage photo-excited carriers' separation and transfer. The experimental data show that MCN-2 has a good quasi-first-order kinetic rate constant k (0.041 min^{-1}) in the photodegradation process of TC driven by visible light. Under the irradiation of visible light, more electrons in VB on the surface of MCN-2 can be excited into CB, thus forming more photoexcited electron-hole pairs (e^--h^+). In addition, all active substances (•O_2, •OH, $^1O_2$, h^+) rapidly attack TC molecules and mineralize into CO_2, H_2O and small molecular intermediates.

In the photocatalytic reaction, the isolated M−N_X sites directly capture photogenerated electrons, while the surrounding non-metallic atoms have photogenerated holes, which synergically promote the separation of photogenerated charge carriers, thus promoting the photocatalytic activity. Single atom Ni/S co-doped g-C_3N_4 was created by Xu et al. TC degradation and CO_2 reduction were used to gauge the material's photocatalytic activity. The findings demonstrate that the implantation of single atomic Ni/S sites on carbon nitride nanosheets using double doping and stripping engineering can considerably improve carrier excitation and facilitate the separation and transmission of electron-hole pairs. In turn, these procedures support effective photocatalytic redox reactions. Ni/S-CN-N is stimulated under visible light

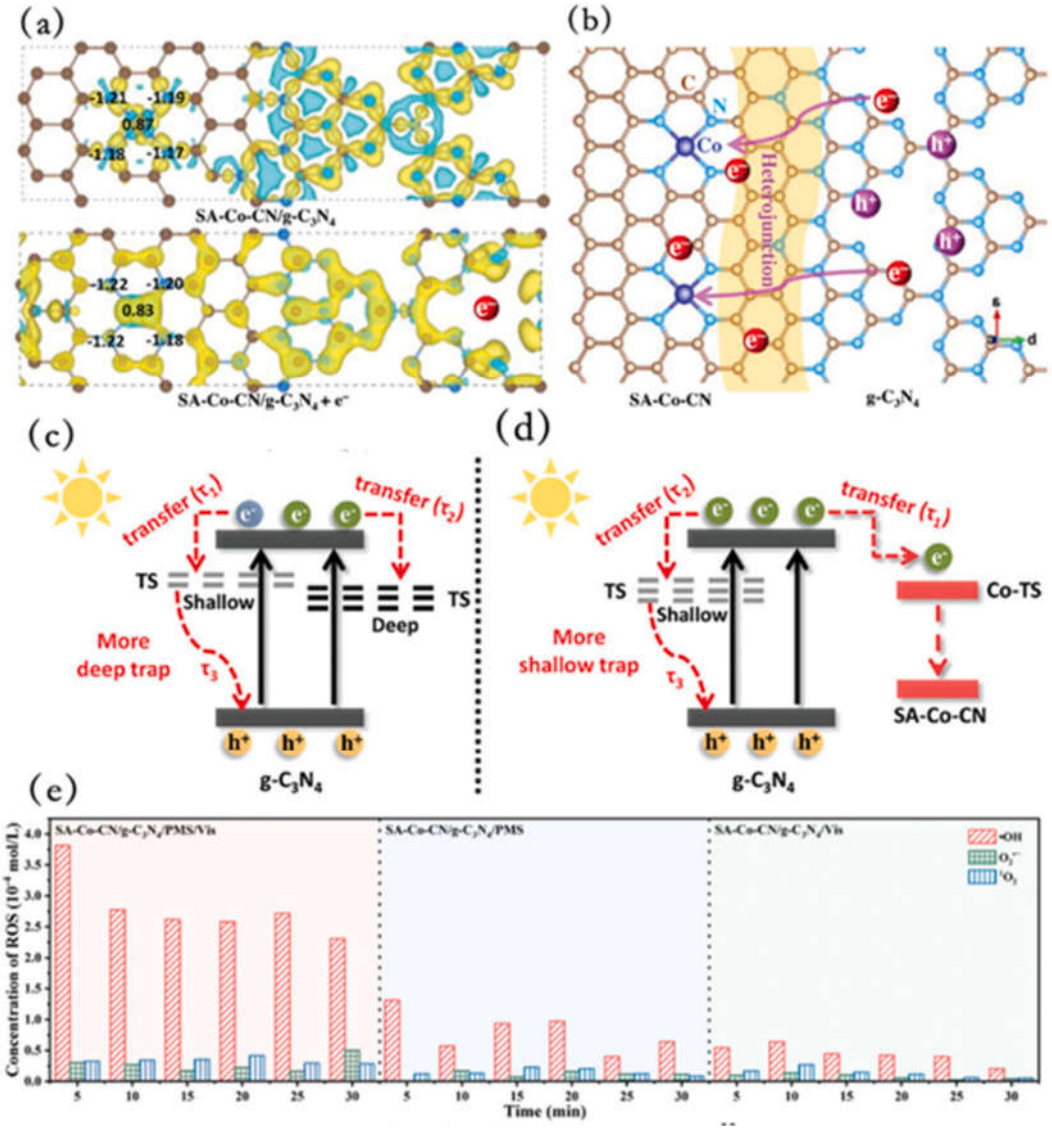

Fig. 7. (a) Bader charge of SA-Co-CN/g-C_3N_4 and SA-Co-CN/g-C_3N_4 upon excitation by one extra e^-; (b) Schematic illustration of the charge transfer between the heterojunction of SA-Co-CN and g-C_3N_4; (c) Schematic representation of proposed charge trapping model in g-C_3N_4, and (d) SA-Co-CN/g-C_3N_4; (e) The yield of ROS of the g-C_3N_4/PMS and SA-Co-CN/g-C_3N_4/ PMS systems [126].

to produce electrons and holes. Then, through the Ni-N/O connection, the electrons move to the Ni site. The molecule O_2 is converted to $^{\bullet}O_2$ by the electrons at the Ni site. Additionally, $^{\bullet}O_2$ and holes can combine to generate $^1O_2$. The presence of H_2O_2 in the TC solution suggests that electrons may have reduced some $^{\bullet}O_2$ or O_2 to H_2O_2, which may then have resolved to $^{\bullet}OH$. As a result, the TC molecules undergo a reaction with the holes, $^{\bullet}O_2$, $^1O_2$, and $^{\bullet}OH$, leading to their degradation. After secondary calcination and Ni/S co-doping, TC's degradation efficiency is increased in comparison to CN.

$$Ni/S-CN-N + hv \rightarrow hole + electron \quad (17)$$

$$Electron + O_2 \rightarrow \cdot O_2 \quad (18)$$

$$\cdot O_2 + hole \rightarrow {}^1O_2 \quad (19)$$

$$O_2 + 2H^+ + 2electron \rightarrow H_2O_2 \quad (20)$$

$$\cdot O_2 + 2H^+ + electron \rightarrow H_2O_2 \quad (21)$$

$$H_2O_2 + H^+ + electron \rightarrow H_2O + \cdot OH \quad (22)$$

$$^1O_2/\cdot O_2 \,/\, hole/\cdot OH + TC \rightarrow degraded \quad product \quad (23)$$

The activity of heterogeneous photocatalytic H_2O_2 activation in Fenton-like processes is strongly correlated with the local electron density of the reaction center atoms. Fe SACs prepared by Su et al. can effectively remove ciprofloxacin (CIP) in a Fenton-like system [130]. Numerous refractory organic pollutants, such as ofloxacin, norfloxacin, tetracycline, and levofloxacin, can be broken down by the Fe_1-Nv/CN/H_2O_2 system. For the cleanup of organic pollutants in water, the innovative system exhibits a remarkable activity and adaptability. According to calculations, the pseudo-first-order kinetic constant (k) of CIP degradation on Fe_1/CN is 0.02211 min^{-1}. Compared to CN and Nv/CN, the Fe_1-Nv/CN exhibits the highest activity. The production of $^{\bullet}OH$, superoxide radicals (O^{2-}), and holes (h^+) can all be precisely inhibited by the reaction system. The $^{\bullet}OH$ is the primary ROS (Fig. 8 a-d). The single-atom material transfers electrons to the Fe single-atom through the substrate carbon nitride under light, thus generating free radicals [130,131]. Moreover, the contribution of photogenerated e^- and h^+ in the photocatalytic process to the enhancement of the catalyst's catalytic activity in the activation of PMS. Under visible light, Fe-g-C_3N_4 degrades

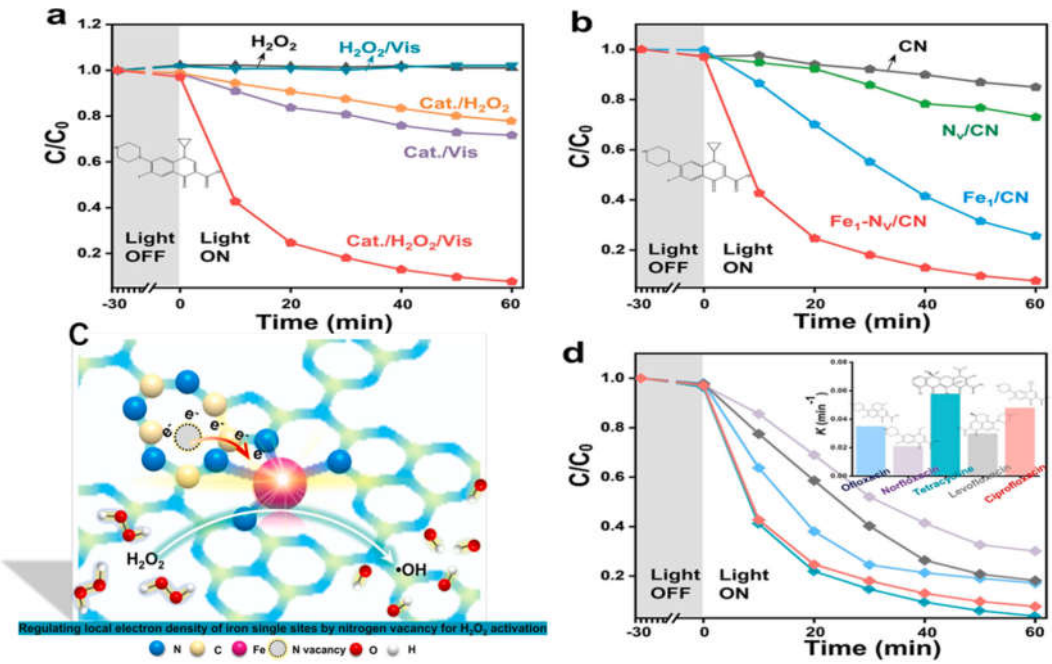

Fig. 8. (a) CIP degradation curves under a photocatalytic process; (b) CIP Degradation curves of CN, Nv/CN, Fe_1/CN and Fe_1-N_v/CN catalyst during photocatalytic activation H_2O_2 process; (c) Schematic illustration of the charge transfer between the system; (d) Degradation of diverse pollutants in the Fe_1-N_v/CN/H_2O_2/Vis system [130].

SMX rapidly by 98.7 % in 6 min [132]. The P-Fe_1Co_1/CN prepared by Yu et al. significantly affects the degradation of pollutant TBBPA under visible light irradiation. Under visible light irradiation, P-Fe_1Co_1/CN shows better degradation efficiency (96 %) in 120 min. Quenching research shows that $•O_2^-$, a photogenerated electron and a hole are key factors in TBBPA debromination. The presence of these active species is demonstrated by the ESR spectra.

4.2. Fenton-like reactions

In recent years, the degradation of organic pollutants by persulfate (PS) in advanced oxidation systems has been extensively studied. Transition metals have been studied as powerful activators for permonosulfate (PMS), peroxydisulphate (PDS), hydrogen peroxide (H_2O_2), and ozone to generate sulfate radical ($SO_4•^-$), hydroxyl radical •OH or superoxide radical ($O_2•^-$), $^1O_2$, high-valent metal species and etc. These free radicals play an essential role in removing pollutants [133,134]. Different single transition metal active sites are fixed on carbon nitride to form SACs for PMS activation. The catalytic formation of free and non-free radicals by single atom metal sites and non-metallic active species inherent in carbon carriers are used to degrade refractory organic pollutants. Various metal centers will initiate different persulfate activation pathways with varying coordination configurations, such as accessible radical pathway, non-free radical pathway or a combination of both. Accessible radical pathway and non-free radical pathway have their advantages. AOPs based on free radicals may be more proper for oxidizing persistent pollutants in relatively clean water substrates. In contrast, non-free radical oxidation may be more suitable for treating contaminants in complex water substrates easily affected by $^1O_2$, electron transfer mediated by a catalyst or high-valent metal species. The combination of the two approaches may be better. In addition, in the materials formed by transition metal and carbon nitride, Lewis base sites will be generated around nitrogen, which can combine with transition metal atoms to form strong M−N (M refers to metal Fe, Co, Mn, Cu, Ni, etc.) sites in the carbon matrix. In addition, the tetra nitrogen coordination transition metal (M−N_4) configuration in SACs plays a key role in optimizing electron transfer in PMS activation [92].

Through experiments and DFT calculations, According to Yang et al., the moderately energetic atomically distributed metal-nitrogen active sites are essential for allowing electron transport for PMS activation. This Mn single-atom catalyst has MnN_4 site, which can catalyze PMS to generate •OH and $SO_4•^-$ free radicals. They also discovered that the target pollutant's adsorption site is pyrrole N. BPA removal by Mn-SAs/CN gained nearly 100 %. The combination of adsorption sites and free radicals improves the catalytic efficiency. Isolated atomic Mn sites play a critical role in activating the PMS required for the high effective degradation of BPA. The higher the adsorption efficiency of BPA, the higher the catalytic activity. Mn SACs superior catalytic performance is attributed to the synergistic effect between the adsorption of the pollutant and the activation of the PMS.

Similarly, Peng et al. found that Fe atoms and pyridinic N in g-C_3N_4 formed Fe-N_x sites. The group of PMS and g-C_3N_4 mainly produces $^1O_2$ in the reaction process. High-valent iron-oxo species might be created when the O atom in the peroxide bond of PMS activation interacted with the Fe(III) species at the atomically dispersed Fe-N_4 sites. As a result, the nearby Fe^{IV} = O, which can be transformed to Fe(III) species, oxidized the adsorbed TC. The nonradical process of TC breakdown employing SA Fe-g-C_3N_4 activated PMS, with high-valent iron-oxo species being the main ROS. The material degrades TC by more than 90 %. The Fe/CN prepared by Zhang et al. generates 100 % $^1O_2$ by activating PMS. It showed high efficiency of chlorophenol (4-CP) degradation [135]. The tendency of Fe/CN to adsorb PMS's O site on the Fe site encourages PMS's oxidation to $SO_5•^-$ by losing the H atom. In addition, $SO_5•^-$ rapidly self-reaction to generate $S_2O_8^{2-}$, SO_4^{2-}, and $^1O_2$. Fe-dispersed g-C_3N_4 catalyst with a Fe-N_4 coordination structure was created by Zhao et al. for the degradation of sulfamethoxazole (SMX) and photocatalytic activation of PMS [132]. The degradation rate of SMX reached 98.7 %. The main reactive species that contribute to the degradation of SMX are •OH, $SO_4•^-$, $O_2•^-$, h^+, $^1O_2$, and Fe^{IV} = O.

In addition, as PMS activators for the breakdown of bisphenol A (BPA), Co single-atom catalysts supported by graphitic carbon nitride (SA-Co-CN) with Co-N_4 active sites were created. Under acidic and alkaline circumstances, high-valent cobalt [Co(IV)] and singlet oxygen ($^1O_2$), respectively, are the primary reactive species of pollution

degradation. According to DFT studies, Co-N_4 structure was adsorbed with the PMS O-O band. The preferred route for PMS is the adsorption of the Co atom and O atom on the O-O bond. Co (IV) = O structure is formed under acidic conditions, and $O_2^{\bullet-}$ is generated under alkaline conditions. Both substances play a crucial role. The results demonstrated that 0.1 g/L of SA-Co-CN in the presence of PMS eliminated 100 % of the BPA in 40 min. It is worth mentioning that the following pathways typically generate $^1O_2$ self-decomposition of PMS ($HSO_5^- + SO_5^{2-} \rightarrow HSO_4^- + SO_4^{2-} + {}^1O_2$), recombination of $O_2^{\bullet-}$ [136], or O_2 for energy transfer [137]. The PMS activation mechanism of the Co SACs prepared by Wu et al. using Vitamin B12 is the synergy of CoO, Co-N and modified g-C_3N_4. Specifically, the modified g-C_3N_4 is mainly responsible for the non-free radical path. At the same time, pathways of the active cobalt site are mainly responsible for the free radical and high-valent cobalt. The coordination number's modification can adjust the electron density of the Co single atom, thereby changing the electron distribution of the C atom adjacent to pyridine N. The Co single atom's charge density determines the catalyst's Fenton-like reaction performance [138]. Wang et al. prepared N, O- coordination Co SACs isolated on oxygen-doped tubular carbon nitride as effective activators of PMS-AOPs [139]. It was found that Co nucleation was mainly at N, O double correlation sites. Co-N_3O_1-Co has a highly oxidized cobalt atomic center, and this structure can adjust the coordination environment and carrier structure. Co-N_3O_1 samples showed a higher catalytic degradation rate. Compared with Co-N, K_{obs} of Co-N_3O_1 increased from 0.0289 min^{-1} to 0.287 min^{-1}. $^1O_2$ was found to be a dominant free radical in Co-N_3O_1/PMS system. In addition, membrane technology was introduced in this study to form a PVDF/Co/PMS system, which has good leaching resistance and mineralization ability.

Furthermore, Miao et al. have demonstrated that the nitrogen coordinated Mn (MnN_5) site is more effective in activating PMS than the MnN_4 site, encouraging the O-O bond to split into high-valent Mn (IV)-oxo species with selectivity close to 100 %. An Mn (IV)-oxo-predominant route was used for PMS activation over MnN_5. The catalytic effect of single oxygen in this system is very small. M−N_5 can remove various refractory pollutants such as phenol, BPA, sulfathiazole and SMX through effective PMS activation. Single atom Cu (SA-Cu) supported on reduced graphene oxide (rGO) was created by Chen et al. The SA-Cu/exposed rGO's single atom Cu sites helped to effectively activate PMS. The degradation rate of SMX in the SA-Cu/rGO/PMS system is 3.9 times more than in rGO/PMS system. In addition, the system can eliminate 99 % of TOC in 2 h. Unlike rGO/PMS system, SA-Cu/rGO/PMS system can produce $^1O_2$ during catalytic activation. The very effective mineralization and degradation of SMX are caused by all the reactive $SO^{\bullet-}$, $^{\bullet}OH$, and $^1O_2$ species cultivated in the SA-Cu/rGO/PMS system.

$$\equiv Cu^+ + HSO_5^- \rightarrow \equiv Cu^{2+} + SO_4^{\cdot-} + OH^- \quad (24)$$

$$\equiv Cu^{2+} + HSO_5^- \rightarrow \equiv Cu^+ + SO_5^{\cdot-} + H^+ \quad (25)$$

$$SO_4^{\cdot-} + H_2O \rightarrow SO_4^{2-} + \cdot OH + H^+ \quad (26)$$

$$HSO_5^- + SO_5^{2-} \rightarrow SO_4^{2-} + HSO_4^- + {}^1O_2 \quad (27)$$

$$2SO_5^{\cdot-} + H_2O \rightarrow 2HSO_4^- + 1.5\,{}^1O_2 \quad (28)$$

$$SO_4^{\cdot-} + \cdot OH + {}^1O_2 + SMX \rightarrow intermediates \rightarrow CO_2 + H_2O \quad (29)$$

In addition to changing the type of metal atoms, adjusting the electronic characteristics of the central atom can also design non-metallic particles on the carbon matrix. Improving SACs activity can cut the coordination structure of metal centers in various ways, enrich the concentration of metal centers, and design the electronic system and porosity of substrates [140]. Pan et al. anchored the dispersed Co on the polymer-derived hollow n-doped porous material [141]. By changing the type or type of heteroatoms, the coordination environment of SACs can be improved, thus improving the activity and selectivity of the catalyst. Zhou et al. prepared Fe SACs loaded on an oxygen-doped nitrogen-rich carbon carrier (SAFe-OCN) and degraded pollutants by activating PMS. Compared with FeN_4, FeN_xO_{4x} is an excellent multi-electron donor and may quickly form high-valent iron during oxidation, the SAFe-OCN increased the phenol degradation kinetics by 5.13 times, and the degradation efficiency of phenol reached 99.3 %. Loading atomic-dispersed Fe onto the OCN carrier can adjust the electronic structure and conductivity of SAFe-OCN, promote the adsorption of PMS and pollutants on the catalyst, and boost the electron transfer pathway. Oxygen-doped g-C_3N_4 (O-g-C_3N_4) can be converted into nitrogen–oxygen co-doped carbon materials by pyrolysis under N_2. N-O co-doped carbon compounds show better catalytic activity as compared to nitrogen-doped carbon materials [142]. Wang et al. created catalysts with the Fe-based dual active site that included Fe_2N and single atom Fe were embedded in graphitic carbon that was co-doped with nitrogen and oxygen. Dual-active sites play a vital role in the activation of PMS. Because the Fe(III) cycle to Fe(II) could be accelerated by using co-doped graphitic carbon as a substrate, Fe-N-O-GC exhibited better catalytic activity and stability. The results showed that the TOC removal rates of various pollutants (bisphenol A, phenol, nitrophenol, nitrobenzene and atrazine) were 72.1 %, 50.8 %, 44.6 %, 11.6 % and 10.4 %, respectively.

In recent years, studies have found that bimetallic active sites can effectively activate peroxydisulfate (PDS) to degrade pollutants. PDS is a symmetrical structure that also contains O-O bonds, but is more stable than PMS because of its bonding ability, so PDS activates and breaks its O-O bonds by energy transfer [143]. Wang et al prepared iron and copper DACs has good degradation effect on tetrabromobisphenol S (TBBPS) by catalyzing PDS [144]. The findings demonstrate that while Cu doping creates adsorption sites for carbon-based materials, Fe doping lowers the electrical impedance. These two methods can both significantly increase the number of active sites. The synergistic effect of Fe and Cu co-doping can improve the electronic structure of N-doped carbon materials and thus improve their participation in the electron transfer process. Double Fe-Cu sites appear to be active sites for PDS activation based on changes in the Fe and Cu valence states during the process. The complex of FeCu DACs and PDS may be the main factor in TBBPS degradation after receiving electrons from TBBPS. Free radicals, $^1O_2$, and high metal species play a secondary role in the degradation of TBBPS. Moreover, it has been found that the introduction of FeCu DACs can optimize the activation of PDS. As shown in Fig. 9 a-c, it is found through DFT calculation that the adsorption energy of diatom is lower than that of single atom, which is more conducive to the adsorption of PDS. Charge density and partial state density analysis (PDOS) show that the chemical bonds formed by dual atom are stronger, and electron transfer from Cu to Fe optimizes the bonding orbital distribution of Fe 3d orbitals [145]. During the activation of PDS, $^{\bullet}OH$, $SO_4^{\bullet-}$, $O_2^{\bullet-}$, and $^1O_2$ can be produced, including free radical and non-free radical mechanisms to catalyze the degradation of target matter. The activation mechanism of PDS is similar to that of PMS, except that PDS is more stable.

In addition, studies have found that the metal loading rate and specific surface area size are not enough to affect the degradation efficiency of pollutants. The unusual reconstruction of spin states on FeCo-N/C improves the electron structure of Fe and Co in the d orbitals, and thus shows the excellent catalytic activity of PMS activation on single-atom Co-N/C and Fe-N/C. The composition of natural water is complex, and there are a large number of inorganic ions, which may have a certain impact on the catalytic efficiency of the catalytic system. Humic acid (HA) is a typical organic natural substance. In the FeCu-N-C/PDS system, the competition between HA and TBBPS for the active sites on the surface of Fe decreases the degradation efficiency of TBBPS. Some studies have found that Cl^- and HCO_3^- have a significant inhibitory effect in the Co-CN/PMS/Light system, a common phenomenon observed in the free radical-dominated system because the pollutants and inorganic anions compete to consume free radicals. Therefore, a non-free radical Co-CN/PMS system has apparent advantages in treating pollutants under complex water substrates.

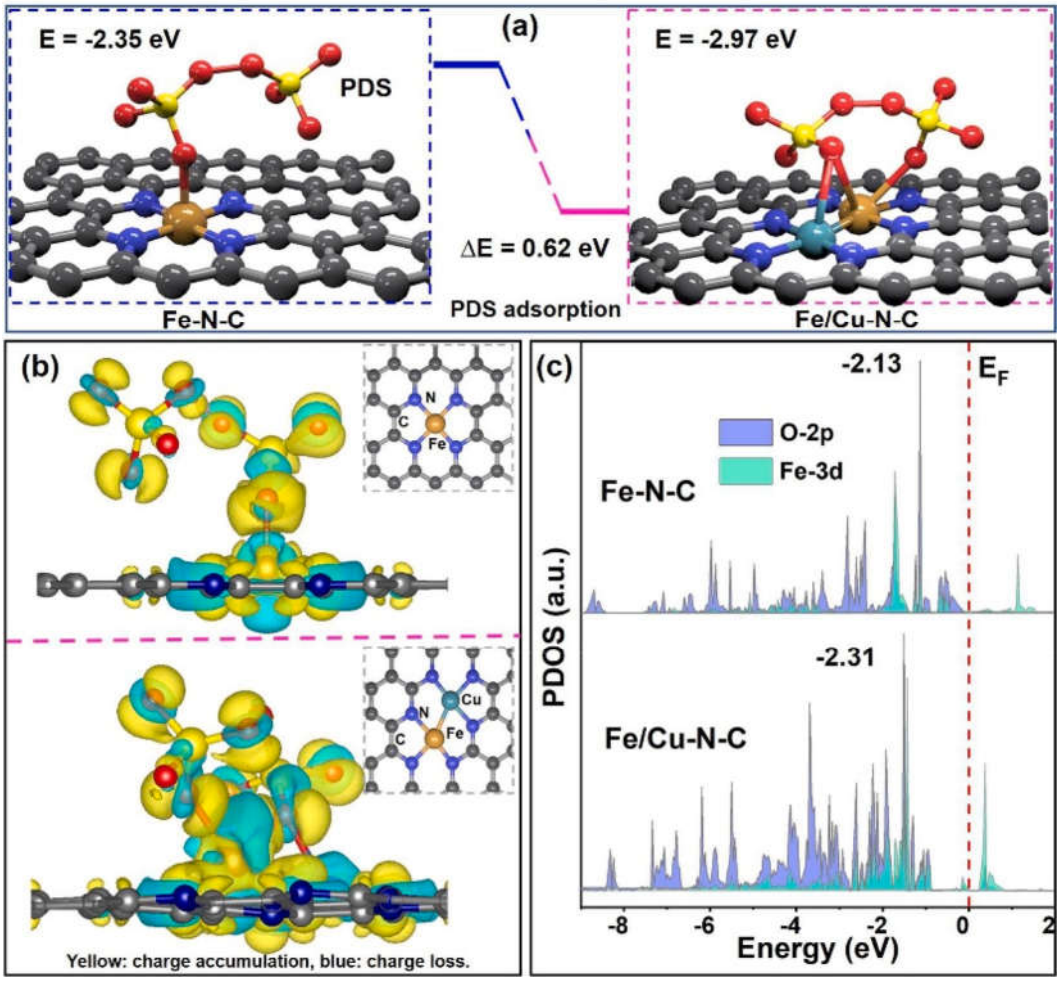

Fig. 9. Differences in the (a) free energy and (b) charge density of PDS adsorbing onto Fe–N–C and Fe/Cu–N–C; and (c) PDOS values calculated for the O–2p and Fe–3d orbitals in Fe–N–C and Fe/Cu–N–C [145].

ADCs by catalytic decomposition of H_2O_2 to produce •OH for pollutant degradation. Ma et al. prepared Mn SACs with dicyandiamide and manganese chloride. It was found by XPS that the binding energy of pyridine C and pyrrole C was reduced by the introduction of Mn single atom, and the Mn single atom was fixed by the nitrogen atom with the coordination bond. The mass fraction of Mn was found by ICP-OES to be 5.2 %. H_2O_2 is adsorbed at Mn-N site to form HOO-Mn-N_4, and a series of REDOX reactions occur, and finally •OH is formed (Fig. 10 a). The catalyst also showed high stability [146]. In addition, Cui et al. prepared Cu SACs by calcination and discovered Cu-O coordination by Cu EXAFS. The material can degrade almost all RhB within five min by activating H_2O_2 to produce •OH, and they designed Fenton filter, which has practical application value (Fig. 10 b-d) [82].

We mainly discuss the application of ADCs to environmental catalysis through photocatalysis and Fenton-like catalysis. In photocatalysis, transition metal atoms are incorporated into carbon nitride, which reduces the bandgap energy of catalyst, increases the absorption of visible light and accelerates the electron transfer. In addition, the interaction of the metal with the g-C_3N_4 carrier improves charge separation. Various active substances produced can selectively catalyze the degradation of pollutants. The performance of ADCs through H_2O_2, PMS and PDS AOPs systems is mainly discussed. The metal site of ADCs can adsorb the target degradation substance and then react with the activated substance. At the same time, there are various mechanisms in the AOPs system of PMS and PDS, including free radical pathway and non-free radical pathway, the former is mainly to produce a variety of free radical further reaction, the latter is mainly to produce catalyst and active agent complex, singlet oxygen and hypervalent species further reaction. The metal single atomic sites of g-C_3N_4 based ADCs, g-C_3N_4 matrix and their interaction together determine the geometric and electronic properties of the catalyst, and further affect its catalytic performance.

4.3. *Electrocatalysis*

The precise atom-level control characteristics of ADCs give these catalysts the advantages of high activity, high stability, and selectivity. The single-atom-carrier interactions and unsaturated coordination environments in ADCs enhance the electrocatalytic performance and contribute to the lowering of the electrochemical reaction energy barrier [148,149]. ADCs can degrade pollutants in water by electrocatalytic oxidative reduction. Wang et al. prepared a Co single-atom-loaded graphene sulfide (Co-SG) catalyst as the cathode electrode material for electrochemical dechlorination by electrochemical reduction of H_2O and atomic hydrogen generated from hydrogen electrolysis. The system not only achieved a degradation rate of 91.1 % for 2,4-dichlorobenzoic acid, but also significantly reduced the TOC concentration by 80 % [150]. Hong et al. prepared Cu single-atom and nitrogen co-doped graphene (Cu@NG) catalysts as electrocatalytic anodes. The system could generate $O_2^{\bullet -}$ to degrade acetaminophen during the electrocatalytic degradation process, achieving a degradation efficiency of 100 % within 90 min while maintaining a low leaching rate of metal ions [151]. In addition, the Ni-Fe dual-atom nitrogen-doped carbon

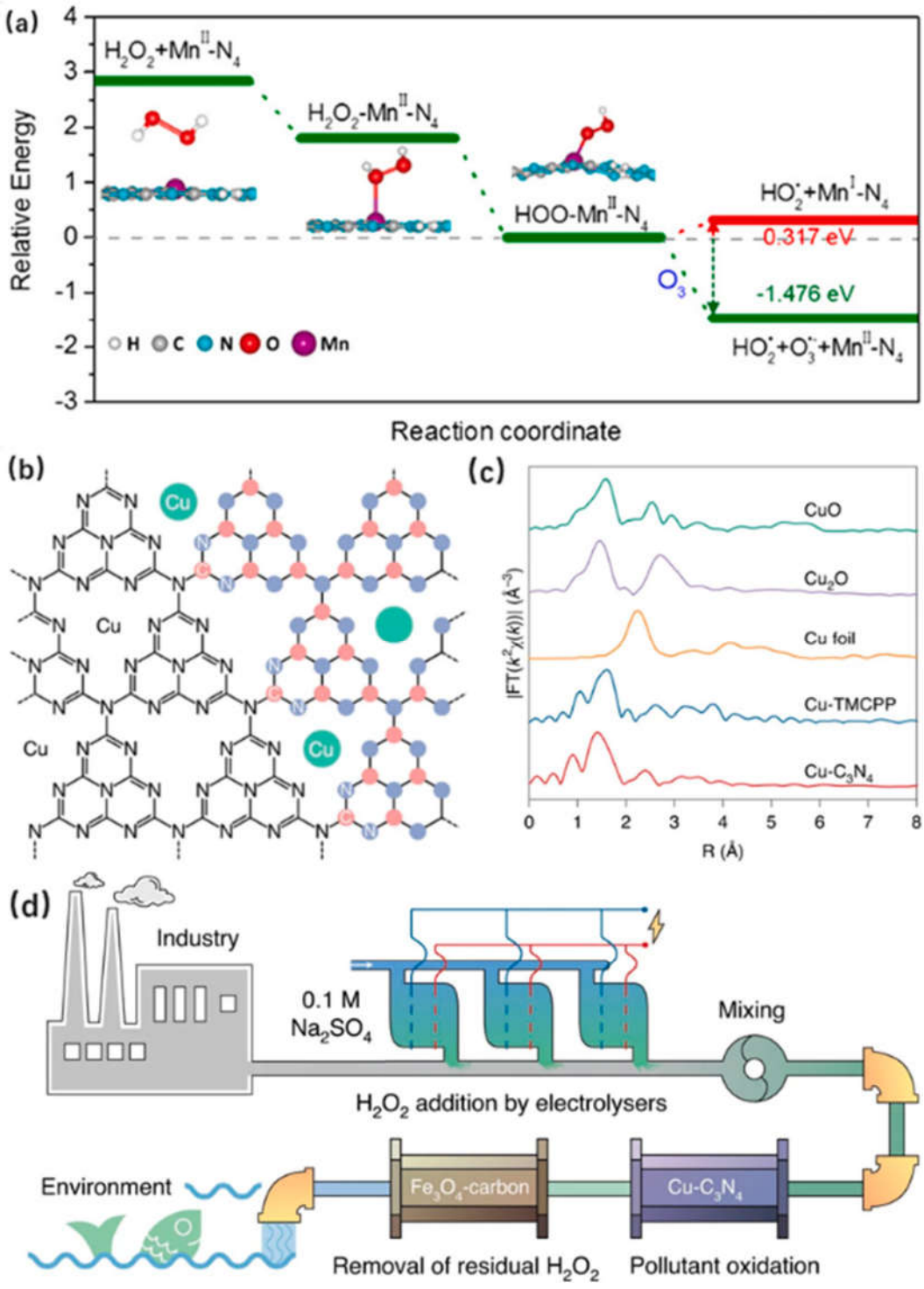

Fig. 10. (a) Free energy of H_2O_2 adsorption and HOO–Mn–N_4 detachment [147]; (b) Structural illustration of Cu-C_3N_4; (c) Structural illustration of Cu-C_3N_4; (d) The system includes the H_2O_2 electrolyser, the Fenton filter and the Fe_3O_4-carbon filter [82].

electrocatalyst ($Ni_{0.5}$-$Fe_{0.5}$-NC) prepared by Liu et al. displayed a 3-electron ORR pathway and efficient production of hydroxyl groups for the degradation of pollutants [152]. Electrocatalytic nitrate reduction using SACs to produce ammonia or nitrogen has also been extensively studied in the field of environment and energy [153]. The Fe single-atom loaded nitrogen-doped carbon (Fe-CNS) catalyst prepared by Li et al. enabled nitrate removal up to 7822 mg $N{\bullet}g^{-1}$ Fe by electrocatalytic reduction. And the ammonia efficiency of this system reached 78.4 % and the nitrogen selectivity of S-modified Fe SACs was 100 % [154].

ADCs with ultra-high atomic utilization efficiency can improve the performance of electrode materials in energy storage devices. Lithium (Li) batteries are the mainstream batteries in current energy storage systems. There have been many studies applying ADCs to Li batteries and obtaining significant results. Liu et al. prepared Co single-atom-anchored ADCs on nitrogen-carbon nanosheets-carbon brazing wafers (CC@CN-SACo) as electrode materials. The hybridized two-dimensional carbon planes formed by the Co sites of this electrode and the substrate provided Li with fast transfer kinetics to form a more uniform Li coating.

The cell not only has an ultra-long cycle life but also has excellent catalytic performance [155]. In addition, lithium-sulfur (Li-S) batteries with high energy density advantage have been widely studied. However, there are still problems such as shuttle effects and lithium dendrite formation that limit their performance. The growth of lithium dendrites can be inhibited by a diaphragm modification strategy [156]. Moreover, materials rich in polar groups (e.g., quantum dots, hydroxyl groups, etc.) or heteroatoms can limit the shuttle effect through the polar sites compared to non-polar pure carbon-based materials [157,158]. SACs can improve the adsorption of soluble and insoluble lithium polysulfides (LiPSs) on the catalyst surface by introducing metal single-atom as the main body of the S, thus inhibiting the shuttle effect. The electrode materials of Co single-atom-loaded nitrogen-doped hollow carbon spheres (ACo@HCS) for ADCs developed by Liu et al. can not only limit the shuttle effect during the catalytic process, but also promote the kinetics of redox reactions. It also exhibits high discharge capacity [159].

5. Stability of atomically dispersed catalysts

The metal active center and coordination environment of single-atom materials have important effects on the activity and stability of catalysts. Extremely even dispersion on the substrate is an important characteristic of a single stable atom. The high dispersion of M−N_x sites in the carbon skeleton is an important element for the high activity and stability of the catalyst, thus reducing the amount metal atoms leached. The reason why g-C_3N_4 is a suitable carrier for atomically dispersed catalysts is that it has a lot of regularly spaced N atoms that can provide anchor points for metal atoms. At the same time, the N atom has a high electronegativity, reflecting the disadvantage of affecting the stability of atomically dispersed catalysts. Through previous studies, it was found that the reduction of stability and catalytic activity of atomically dispersed catalysts was mainly due to the removal of metal atoms during the use of materials. The main criteria to judge the stability of a catalyst are metal ion leaching rate, the change of the structure before and after the recycling of the catalyst, the removal rate of TOC and pollutants and so on.

Mn-SACs prepared by Mao et al. have good stability [161]. The high-resolution C 1 s spectra for both new and used Mn-CNH show no new peaks, but the N 1 s spectra show a new peak with a similar peak size at about 399 eV, which is indicative of the metal-nitrogen coordination. Mn still has high catalytic degradation performance after five cycles of testing, and the metal ion leaching rate is low. In addition, SMX, ciprofloxacin (CIP), RhB, and methyl orange are just a few examples of the numerous organic micropollutants that Mn-CNH effectively removes at a high removal rate. Notably, the rate of TC breakdown in water is unaffected by the addition of common background contaminants like HA, OA, Cl^-, and HCO_3^-, as well as in running water and river water (Fig. 11 a-f).

Wang et al. conducted five consecutive BPA removal tests on SA-Co-CNs to estimate the recoverability of the catalyst. Under acidic conditions, the catalyst degrades BPA for five consecutive times, resulting in a reduction in Co content and a significant reduction in pollutant removal

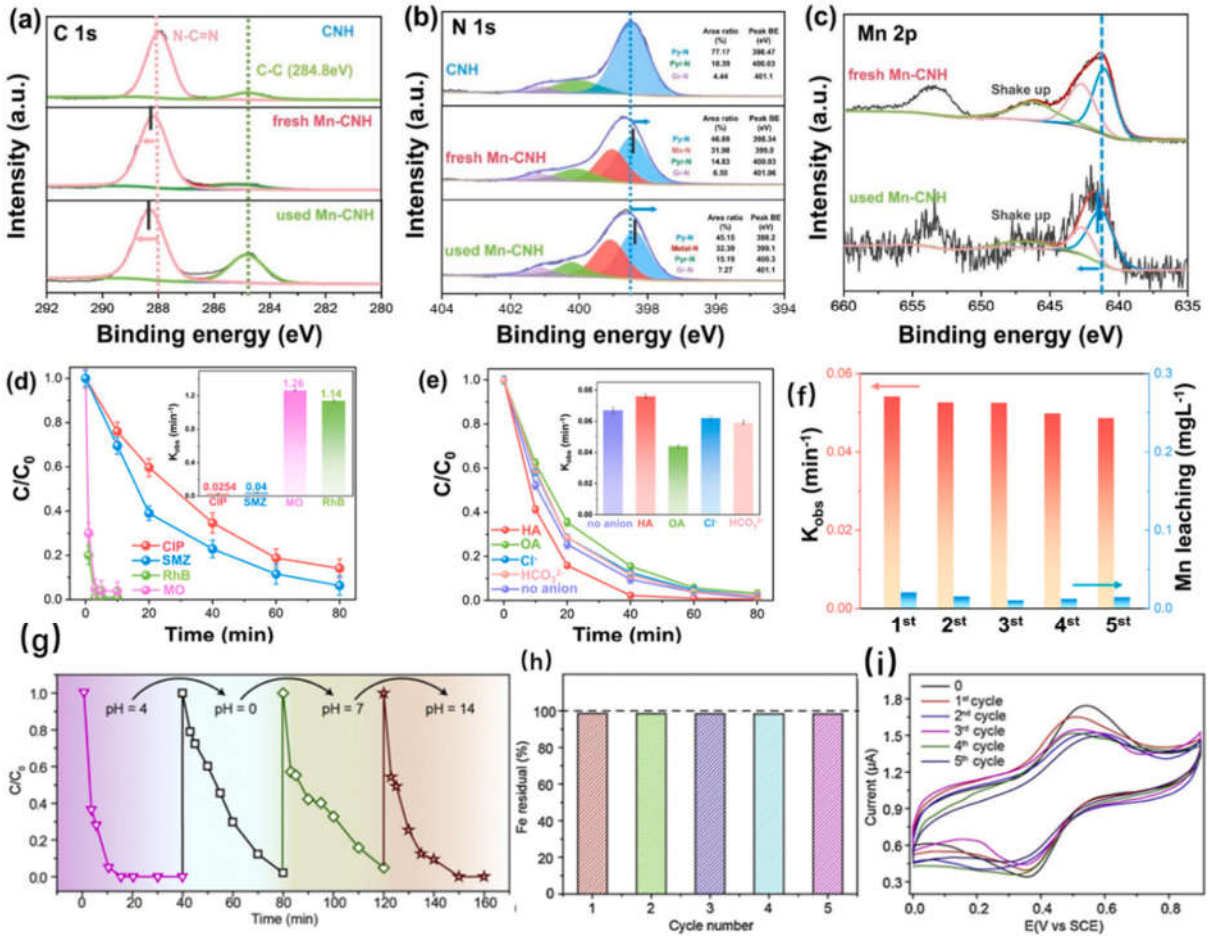

Fig. 11. The C 1 s (a) and N 1 s (b) spectra of g-CNH, fresh Mn-CNH, and used Mn-CNH; (c) Mn 2p spectra of fresh and used Mn-CNH; (d) The capability of the Mn-CNH/Fe/H_2O_2 system for degrading various pollutants; (e) Effect of anion on TC removal in the Mn-CNH/Fe/H_2O_2 system; (f) Reusability tests of Mn-CNH and Fe leaching during successive five-time runs [161]; (g) The degradation performance during cycles of solution with different pH conditions, with C_3N_4-Fe-rGO as the catalyst; (h) ass ratio in the catalyst after each round; (i) CV curves measurement of C_3N_4-Fe-rGO composite after each time Fenton-like reaction [162].

efficiency. However, under alkaline conditions, the removal efficiency changes little. This kind of Co single-atom material has high recyclability. Wang et al. found in the circulation experiment that the pollutants were completely removed after five treatments and reflected the excellent stability of the catalyst. In addition, the metal leaching of the catalyst may have a certain impact on removing pollutants. An et al. found that the MB removal rate of FeN_x/g-C_3N_4 material can reach about 98 % in 15 min after four cycles of experiments. At neutral pH, catalysis of dissolved iron ions in a uniform manner has little contribution to the total amount of organic degradation [160]. The single-atom Mn material with carbon nitride as the carbon matrix shows excellent catalytic performance in removing pollutants. Yang et al. conducted stability tests on this kind of material. In the catalytic performance test of different pH solutions, it is found that when the pH is lower than 8.5, Mn-SAs/CN has 100 % degradation of BPA was observed in 6 min. BPA could still degrade 100 % in 10 min under pH = 10.5, indicating high Fenton-like catalytic stability. The recovery experiment found that the degradation rate of BPA was basically unchanged in the four cycles. After two rounds of a Fenton-like reaction, the leaching concentration of Mn is very small, which can effectively avoid secondary pollution caused by metal leaching in the reaction. In addition, the leached manganese ion can also trigger PMS to oxidize pollutants. It was found that the degradation rate of BPA can attain 7 % with manganese ions as catalysts. The MnN_5/PMS system is efficient for the removal of 4-CP. After six consecutive catalytic recycles, MnN_5 still had a high level of activity. In addition, MnN_5 also showed efficient catalytic performance in a complex aqueous matrix, achieving 100 % 4-CP removal in 15 min.

To ensure the strong coordination between metal sites and carbon nitride in ADCs is the key to maintain the high stability of materials. By improving the structure of the material, it can anchor the metal atoms more stably and prevent ROS from destroying the material. Wang et al. prepared an “Oreo-like” structure of ADCs with carbon nitride as a carrier, dispersing Fe single atom between the two [162]. Such a layered structure can not only prevent the leaching and aggregation of Fe single atom, but also maintain high activity under extreme pH conditions, greatly reducing the damage degree of ROS to the catalyst. The material has been degraded several times at different pH values. By comparing the data of different materials, the Oreo layered structure has a stable catalytic ability in the pH = 0–14 range. In addition, four cycles of experiments were carried out at pH = 4, 0, 7 and 14. The oxidation and reduction potentials of iron sites did not change in the cyclic experiment. It is proved that the double layer structure can stabilize the Fe single atom. (Fig. 11 g-i).

During the recovery of the catalyst, it was found that the catalyst activity could be recovered by heating and regenerating the catalyst. After calcination, the SA Fe-g-C_3N_4 catalyst’s catalytic activity may have recovered as a result of the removal of intermediate products that had become adsorbate on the catalyst’s active core and edge. Shang et al. collected Fe SACs after three degradation experiments and heated them at 350°. The cyclic experiment results showed that the degradation rate of SMX was recovered, indicating that the heat treatment effectively restored the stability. [163]. Similarly, the stability of Cu SA/CNS was tested by cyclic test. After five cycles, it was discovered that neither the photocatalytic activity nor the catalyst’s crystal structure had appreciably decreased. In addition, some researchers have found that the material after leaching metal ions during the cycle experiment has no effect on the degradation of pollutants. For instance, it was found that the leaching concentrations of Co and Fe in the FeCo-N-C/PMS system were 0.06 and 0.13 mg/L, respectively, and only degraded less than 5 % of the phenol in the homogeneous catalytic system.

6. Conclusion and prospect

The rapid progress of ADCs has bridged the relationship between homogeneous and heterogeneous catalysts. The reasonable design of advanced catalysts with high activity and low cost is the key to using advanced oxidation technology to treat contaminants in water. So far, g-C_3N_4-based ADCs been widely employed abundant anchoring sites and strong mutual effect between g-C_3N_4 support and single atom are necessary for obtaining stable g-C_3N_4 based single atom photocatalysts. The unique atomic structure, definite active site and unsaturated coordination environment of metal atoms make them attractive in advanced oxidation techniques. Furthermore, it is found that the DACs can enhance the catalytic efficiency through the synergistic effect of atoms. g-C_3N_4 based ADCs have great prospects in AOPs.

The synthesis methods of g-C_3N_4-based ADCs and their applications in the environmental field are reviewed in this paper. Currently, the design of g-C_3N_4-based ADCs mainly adopts the pyrolysis method combined with other methods, including the ball milling method, physical and chemical precipitation method, etc. The mechanism of pollutant degradation by g-C_3N_4-based ADCs was introduced. In environmental catalytic applications, the g-C_3N_4 substrate and the loaded single atom are interdependent and mutually beneficial. Monatomization is facilitated by the unique geometric and electrical structure of g-C_3N_4, which also inhibits the development of aggregates. In addition, the 2D plane of g-C_3N_4 provides a perfect setting for accelerating the catalytic adsorption and diffusion process, enhancing g-C_3N_4-based ADCs’ activity and stability noticeably. In the advanced oxidation system of g-C_3N_4-based ADCs, combining free radical and non-free radical pathways can improve the catalytic efficiency and mineralization degree of pollutants in wastewater. Although g-C_3N_4-based ADCs have made remarkable achievements in AOPs applications, their theoretical and application-related research faces opportunities and challenges.

1) Although the preparation techniques have been well developed, the controlled design of g-C_3N_4-based SACs remains a huge challenge. We need to ensure that the utilization rate and dispersion of the metal active center can be improved. Low matrix surface area and relatively weak interactions are important elements. A simple strategy for preparing highly loaded single atoms on g-C_3N_4 still needs to be improved. The instability of single atoms and clusters risks grouping together and deactivating active sites. How to increase the single atom load while reasonably dispersive single atom and develop low-cost, time-saving strategies are the main research points. In addition, the diversity and flexibility of the diatomic structure make the dual atom site catalyst have high catalytic performance. However, it is difficult to regulate the structure and uniform dispersion of atoms in the materials during the synthesis of DACs.
2) At present, most studies on carbon nitride groups in advanced oxidation technology focus on metal atom-nitrogen sites and metal atom-carbon sites. Many studies have introduced non-metallic elements doping into SACs to modulate local coordination environment to enhance catalytic performance and stability. Therefore, more and more studies have been conducted on the coordination of metal elements with other nonmetallic atom (such as S, O, P, etc.) in SACs. In addition, DACs also have multiple active centers, and the interaction force between the two metals may impact the support and catalytic system. How to characterize the active center and the electronic structure is a key problem in the study of ADCs, and the electronic structure, active center and catalytic path mechanism of such catalysts still need to be determined.
3) Compared to SACs, DACs are still in their infancy. Further research is needed on how to precisely control the configuration of dual-atom, atomic distances, double-atom loading, and uniform dispersion. Realizing the uniform distribution of dual-atom is of great significance in clarifying the conformational relationship. Moreover, the dual-atom active sites in DACs are difficult to be identified by existing characterization techniques, which hinders the study of the active sites and reaction mechanisms of DACs. It is a major challenge to identify the dynamic changes of chemical valence and coordination environment for DACs.

4) Theoretical calculation has become an important tool for studying the local atom-carrier interaction, coordination environment, electronic structure and charge transfer in the catalytic process of g-C_3N_4-based SACs, which can reveal the working mechanism of SACs in the catalytic reaction. Detailed experimental evidence should be combined with theoretical work to fully understand the metal atom-carbon nitride support interaction and the corresponding complete catalytic mechanism in real-world scenarios. A large amount of data is already available for SACs and DACs, and a well-established and standardized database would be beneficial for the design and application of ADCs. Therefore, the development of machine learning combined with high-throughput calculation to foresee the coordination structure of single atoms in g-C_3N_4 supported SACs and the catalytic activity of carbon nitride supported SACs is conducive to the development of efficient g-C_3N_4-based SACs.
5) g-C_3N_4-based ADCs are mostly used in photocatalysis, including water decomposition, hydrogen evolution reaction, carbon dioxide reduction, nitrogen fixation, redox reaction, etc. Many g-C_3N_4-based ADCs are also widely used in non-photocatalytic AOPs. In addition, many emerging catalytic fields are in their infancy. For example, plasma catalysis and microwave-assisted catalysis, etc. SACs and DACs are expected to realize their potentials in emerging catalytic fields with their own advantages.
6) The practical application of g-C_3N_4-based ADCs in treating environmental pollutants is difficult. True water-based media often contain complex background components (such as poisonous heavy metals, anions, organics, and microorganisms) that may impact the entire advanced oxidation system through ROS consumption, surface contamination, and catalyst deactivation. In addition, ROS destruction of the carbon nitride matrix may affect the stability of the catalyst. Therefore, to assure the high working of catalysts in complicated water environments, better strategies must be explored to design more efficient, reactive and highly selective ADCs. In addition, ADCs can be combined with membrane technology and fixed-bed reactors to enhance the practical application value of ADCs. The realization of large-scale novel ADCs for advanced oxidation is a practical and promising technology.

Declaration of competing interest

The authors declare that they have no known competing financial interests or personal relationships that could have appeared to influence the work reported in this paper.

Data availability

Data will be made available on request.

Acknowledgments

This study was financially supported by the Program for the National Natural Science Foundation of China (52100182, U20A20323, 52300204), the Fundamental Research Funds for the Central Universities (531118010574), the Science and Technology Innovation Program of Hunan Province (2023RC3122) and the Hunan Provincial Natural Science Foundation of China (2022JJ40086, 2023JJ40232).

References

[1] A. Hojjati-Najafabadi, M. Mansoorianfar, T. Liang, K. Shahin, H. Karimi-Maleh, A review on magnetic sensors for monitoring of hazardous pollutants in water resources, Sci. Total Environ. 824 (2022) 153844, https://doi.org/10.1016/j.scitotenv.2022.153844.
[2] A. Saravanan, P. Senthil Kumar, S. Jeevanantham, M. Anubha, S. Jayashree, Degradation of toxic agrochemicals and pharmaceutical pollutants: Effective and alternative approaches toward photocatalysis, Environ. Pollut. (298 2022) 118844, https://doi.org/10.1016/j.envpol.2022.118844.
[3] D.B. Miklos, C. Remy, M. Jekel, K.G. Linden, J.E. Drewes, U. Hübner, Evaluation of advanced oxidation processes for water and wastewater treatment – A critical review, Water Research 139 (2018) 118–131, https://doi.org/10.1016/j.watres.2018.03.042.
[4] W. Xia, B. Song, H. Yi, E. Almatrafi, Y. Yang, Y. Fu, X. Huo, F. Qin, L. Xiang, Y. Zeng, G. Zeng, C. Zhou, From aquatic biota to autogenous N-doping biochar—using a highly efficient nonradical dominant process for sulfamethoxazole degradation, Journal of Cleaner Production 373 (2022) 133750, https://doi.org/10.1016/j.jclepro.2022.133750.
[5] Y.-H. Chuang, S. Chen, C.J. Chinn, W.A. Mitch, Comparing the UV/Monochloramine and UV/Free Chlorine Advanced Oxidation Processes (AOPs) to the UV/Hydrogen Peroxide AOP Under Scenarios Relevant to Potable Reuse, Environ. Sci. Technol. 51 (2017) 13859–13868, https://doi.org/10.1021/acs.est.7b03570.
[6] Z. Yao, M. Wang, R. Jia, Q. Zhao, L. Liu, S. Sun, Comparison of UV-based advanced oxidation processes for the removal of different fractions of NOM from drinking water, J. Environ. Sci. 126 (2023) 387–395, https://doi.org/10.1016/j.jes.2022.03.0401001-0742.
[7] K. Yin, Y. Shang, D. Chen, B. Gao, Q. Yue, X. Xu, Redox potentials of pollutants determining the dominate oxidation pathways in manganese single-atom catalyst (Mn-SAC)/peroxymonosulfate system: Selective catalytic mechanisms for versatile pollutants, Applied Catalysis b: Environmental 338 (2023) 123029, https://doi.org/10.1016/j.apcatb.2023.123029.
[8] X. Zheng, B. Li, Q. Wang, D. Wang, Y. Li, Emerging low-nuclearity supported metal catalysts with atomic level precision for efficient heterogeneous catalysis, Nano Res. 15 (2022) 7806–7839, https://doi.org/10.1007/s12274-022-4429-9.
[9] Y. Wang, X. Zhao, D. Cao, Y. Wang, Y. Zhu, Peroxymonosulfate enhanced visible light photocatalytic degradation bisphenol A by single-atom dispersed Ag mesoporous g-C3N4 hybrid, Applied Catalysis b: Environmental 211 (2017) 79–88, https://doi.org/10.1016/j.apcatb.2017.03.079.
[10] X. Li, X. Huang, S. Xi, S. Miao, J. Ding, W. Cai, S. Liu, X. Yang, H. Yang, J. Gao, J. Wang, Y. Huang, T. Zhang, B. Liu, Single Cobalt Atoms Anchored on Porous N-Doped Graphene with Dual Reaction Sites for Efficient Fenton-like Catalysis, J. Am. Chem. Soc. 140 (2018) 12469–12475, https://doi.org/10.1021/jacs.8b05992.
[11] Z. Wang, Y. Zeng, J. Deng, Z. Wang, Z. Guo, Y. Yang, X. Xu, B. Song, G. Zeng, C. Zhou, Preparation and Application of Single-Atom Cobalt Catalysts in Organic Synthesis and Environmental Remediation, Small Methods n/a (n.d.) 2301363. https://doi.org/10.1002/smtd.202301363.
[12] M. Kohantorabi, G. Moussavi, S. Giannakis, A review of the innovations in metal- and carbon-based catalysts explored for heterogeneous peroxymonosulfate (PMS) activation, with focus on radical vs. non-radical degradation pathways of organic contaminants, Chem. Eng. J. 411 (2021) 127957, https://doi.org/10.1016/j.cej.2020.127957.
[13] X. Cui, W. Li, P. Ryabchuk, K. Junge, M. Beller, Bridging homogeneous and heterogeneous catalysis by heterogeneous single-metal-site catalysts, Nat. Catal. 1 (2018) 385–397, https://doi.org/10.1038/s41929-018-0090-9.
[14] L. Han, H. Cheng, W. Liu, H. Li, P. Ou, R. Lin, H.-T. Wang, C.-W. Pao, A.R. Head, C.-H. Wang, X. Tong, C.-J. Sun, W.-F. Pong, J. Luo, J.-C. Zheng, H.L. Xin, A single-atom library for guided monometallic and concentration-complex multimetallic designs, Nat. Mater. 21 (2022) 681-+, https://doi.org/10.1038/s41563-022-01252-y.
[15] X.-F. Yang, A. Wang, B. Qiao, J. Li, J. Liu, T. Zhang, Single-Atom Catalysts: A New Frontier in Heterogeneous Catalysis, Acc. Chem. Res. 46 (2013) 1740–1748, https://doi.org/10.1021/ar300361m.
[16] J. Yang, D. Zeng, J. Li, L. Dong, W.-J. Ong, Y. He, A highly efficient Fenton-like catalyst based on isolated diatomic Fe-Co anchored on N-doped porous carbon, Chem. Eng. J. 404 (2021) 126376, https://doi.org/10.1016/j.cej.2020.126376.
[17] W. Zhu, L. Zhang, S. Liu, A. Li, X. Yuan, C. Hu, G. Zhang, W. Deng, K. Zang, J. Luo, Y. Zhu, M. Gu, Z.-J. Zhao, J. Gong, Enhanced CO2 Electroreduction on Neighboring Zn/Co Monomers by Electronic Effect, Angewandte Chemie International Edition 59 (2020) 12664–12668, https://doi.org/10.1002/anie.201916218.
[18] S. Tian, B. Wang, W. Gong, Z. He, Q. Xu, W. Chen, Q. Zhang, Y. Zhu, J. Yang, Q. Fu, C. Chen, Y. Bu, L. Gu, X. Sun, H. Zhao, D. Wang, Y. Li, Dual-atom Pt heterogeneous catalyst with excellent catalytic performances for the selective hydrogenation and epoxidation, Nat. Commun. 12 (2021) 3181, https://doi.org/10.1038/s41467-021-23517-x.
[19] J. Wang, Z. Huang, W. Liu, C. Chang, H. Tang, Z. Li, W. Chen, C. Jia, T. Yao, S. Wei, Y. Wu, Y. Lie, Design of N-Coordinated Dual-Metal Sites: A Stable and Active Pt-Free Catalyst for Acidic Oxygen Reduction Reaction, J. Am. Chem. Soc. 139 (2017) 17281–17284, https://doi.org/10.1021/jacs.7b10385.
[20] L. Shi, T. Wang, H. Zhang, K. Chang, J. Ye, Electrostatic Self-Assembly of Nanosized Carbon Nitride Nanosheet onto a Zirconium Metal-Organic Framework for Enhanced Photocatalytic CO2 Reduction, Adv. Funct. Mater. 25 (2015) 5360–5367, https://doi.org/10.1002/adfm.201502253.
[21] C. Zhou, E. Almatrafi, X. Tang, B. Shao, W. Xia, B. Song, W. Xiong, W. Wang, H. Guo, S. Chen, G. Zeng, Investigation on the structure-performance of phthalic acid carboxyl position and carbon nitride towards efficient photocatalytic degradation of organic pollutants, Sep. Purif. Technol. 286 (2022) 120464, https://doi.org/10.1016/j.seppur.2022.120464.
[22] C. He, W. Xia, C. Zhou, D. Huang, C. Zhang, B. Song, Y. Yang, J. Li, X. Xu, Y. Shang, L. Du, Rational design to manganese and oxygen co-doped polymeric carbon nitride for efficient nonradical activation of peroxymonosulfate and the mechanism insight, Chemical Engineering Journal 430 (2022) 132751, https://doi.org/10.1016/j.cej.2021.132751.

[23] C. Zhou, Y. Liang, W. Xia, E. Almatrafi, B. Song, Z. Wang, Y. Zeng, Y. Yang, Y. Shang, C. Wang, G. Zeng, Single atom Mn anchored on N-doped porous carbon derived from spirulina for catalyzed peroxymonosulfate to degradation of emerging organic pollutants, Journal of Hazardous Materials 441 (2023) 129871, https://doi.org/10.1016/j.jhazmat.2022.129871.
[24] Y. Zeng, E. Almatrafi, W. Xia, B. Song, W. Xiong, M. Cheng, Z. Wang, Y. Liang, G. Zeng, C. Zhou, Nitrogen-doped carbon-based single-atom Fe catalysts: Synthesis, properties, and applications in advanced oxidation processes, Coordination Chemistry Reviews 475 (2023) 214874, https://doi.org/10.1016/j.ccr.2022.214874.
[25] Y. Yang, G. Zeng, D. Huang, C. Zhang, D. He, C. Zhou, W. Wang, W. Xiong, B. Song, H. Yi, S. Ye, X. Ren, In Situ Grown Single-Atom Cobalt on Polymeric Carbon Nitride with Bidentate Ligand for Efficient Photocatalytic Degradation of Refractory Antibiotics, Small 16 (2020) 2001634, https://doi.org/10.1002/smll.202001634.
[26] J. Feng, H. Gao, L. Zheng, Z. Chen, S. Zeng, C. Jiang, H. Dong, L. Liu, S. Zhang, X. Zhang, A Mn-N3 single-atom catalyst embedded in graphitic carbon nitride for efficient CO2 electroreduction, Nat Commun 11 (2020) 4341, https://doi.org/10.1038/s41467-020-18143-y.
[27] Y. Hu, Z. Li, B. Li, C. Yu, Recent Progress of Diatomic Catalysts: General Design Fundamentals and Diversified Catalytic Applications, Small 18 (2022) 2203589, https://doi.org/10.1002/smll.202203589.
[28] T. Gan, D. Wang, Atomically dispersed materials: Ideal catalysts in atomic era, Nano Res. (2023), https://doi.org/10.1007/s12274-023-5700-4.
[29] X. Wu, J.-H. Kim, Outlook on Single Atom Catalysts for Persulfate-Based Advanced Oxidation, ACS EST Eng. 2 (2022) 1776–1796, https://doi.org/10.1021/acsestengg.2c00187.
[30] J. Lin, W. Tian, Z. Guan, H. Zhang, X. Duan, H. Wang, H. Sun, Y. Fang, Y. Huang, S. Wang, Functional Carbon Nitride Materials in Photo-Fenton-Like Catalysis for Environmental Remediation, Adv. Funct. Mater. 32 (2022) 2201743, https://doi.org/10.1002/adfm.202201743.
[31] B. Singh, V. Sharma, R.P. Gaikwad, P. Fornasiero, R. Zbořil, M.B. Gawande, Single-Atom Catalysts: A Sustainable Pathway for the Advanced Catalytic Applications, Small 17 (2021) 2006473, https://doi.org/10.1002/smll.202006473.
[32] Z. Liang, J. Shen, X. Xu, F. Li, J. Liu, B. Yuan, Y. Yu, M. Zhu, Advances in the Development of Single-Atom Catalysts for High-Energy-Density Lithium-Sulfur Batteries, Advanced Materials 34 (2022) 2200102, https://doi.org/10.1002/adma.202200102.
[33] H. Li, S. Di, P. Niu, S. Wang, J. Wang, L. Li, A durable half-metallic diatomic catalyst for efficient oxygen reduction, Energy & Environmental Science 15 (2022) 1601–1610, https://doi.org/10.1039/D1EE03194E.
[34] M. Li, J. Chen, W. Wu, S. Wu, L. Xu, S. Dong, Diatomic Fe-Fe catalyst enhances the ability to degrade organic contaminants by nonradical peroxymonosulfate activation system, Nano Res. 16 (2023) 4678–4684, https://doi.org/10.1007/s12274-022-5124-6.
[35] J. Liebig, Uber einige Stickstoff - Verbindungen, Annalen Der Pharmacie 10 (1834) 1–47, https://doi.org/10.1002/jlac.18340100102.
[36] F.K. Kessler, Y. Zheng, D. Schwarz, C. Merschjann, W. Schnick, X. Wang, M. J. Bojdys, Functional carbon nitride materials design strategies for electrochemical devices, Nat. Rev. Mater. 2 (2017) 17030, https://doi.org/10.1038/natrevmats.2017.30.
[37] D.M. Teter, R.J. Hemley, Low-Compressibility Carbon Nitrides, Science 271 (1996) 53–55, https://doi.org/10.1126/science.271.5245.53.
[38] E. Kroke, M. Schwarz, E. Horath-Bordon, P. Kroll, B. Noll, A.D. Norman, Tri-s-triazine derivatives. Part I. From trichloro-tri-s-triazine to graphitic C3N4 structures, New J. Chem. 26 (2002) 508–512, https://doi.org/10.1039/b111062b.
[39] Y. Li, J. Zhang, Q. Wang, Y. Jin, D. Huang, Q. Cui, G. Zou, Nitrogen-Rich Carbon Nitride Hollow Vessels: Synthesis, Characterization, and Their Properties, J. Phys. Chem. B 114 (2010) 9429–9434, https://doi.org/10.1021/jp103729c.
[40] L.-F. Gao, T. Wen, J.-Y. Xu, X.-P. Zhai, M. Zhao, G.-W. Hu, P. Chen, Q. Wang, H.-L. Zhang, Iron-Doped Carbon Nitride-Type Polymers as Homogeneous Organocatalysts for Visible Light-Driven Hydrogen Evolution, ACS Appl. Mater. Interfaces 8 (2016) 617–624, https://doi.org/10.1021/acsami.5b09684.
[41] H. Zhang, W. Tian, X. Duan, H. Sun, Y. Shen, G. Shao, S. Wang, Functional carbon nitride materials for water oxidation: from heteroatom doping to interface engineering, Nanoscale 12 (2020) 6937–6952, https://doi.org/10.1039/D0NR00652A.
[42] M.S. Nasir, G. Yang, I. Ayub, S. Wang, L. Wang, X. Wang, W. Yan, S. Peng, S. Ramakarishna, Recent development in graphitic carbon nitride based photocatalysis for hydrogen generation, Applied Catalysis b: Environmental 257 (2019) 117855, https://doi.org/10.1016/j.apcatb.2019.117855.
[43] F. Dong, Z. Zhao, T. Xiong, Z. Ni, W. Zhang, Y. Sun, W.-K. Ho, In Situ Construction of g-C3N4/g-C3N4 Metal-Free Heterojunction for Enhanced Visible-Light Photocatalysis, ACS Appl. Mater. Interfaces 5 (2013) 11392–11401, https://doi.org/10.1021/am403653a.
[44] T.K.A. Nguyen, T.-T. Pham, H. Nguyen-Phu, E.W. Shin, The effect of graphitic carbon nitride precursors on the photocatalytic dye degradation of water-dispersible graphitic carbon nitride photocatalysts, Applied Surface Science 537 (2021) 148027, https://doi.org/10.1016/j.apsusc.2020.148027.
[45] Y.C. Zhao, D.L. Yu, H.W. Zhou, Y.J. Tian, O. Yanagisawa, Turbostratic carbon nitride prepared by pyrolysis of melamine, J Mater Sci 40 (2005) 2645–2647, https://doi.org/10.1007/s10853-005-2096-3.
[46] D.J. Martin, K. Qiu, S.A. Shevlin, A.D. Handoko, X. Chen, Z. Guo, J. Tang, Highly Efficient Photocatalytic H2 Evolution from Water using Visible Light and Structure-Controlled Graphitic Carbon Nitride, Angewandte Chemie International Edition 53 (2014) 9240–9245, https://doi.org/10.1002/anie.201403375.
[47] S.C. Yan, Z.S. Li, Z.G. Zou, Photodegradation Performance of g-C3N4 Fabricated by Directly Heating Melamine, Langmuir 25 (2009) 10397–10401, https://doi.org/10.1021/la900923z.
[48] H. Montigaud, B. Tanguy, G. Demazeau, I. Alves, S. Courjault, C3N4: Dream or reality? Solvothermal synthesis as macroscopic samples of the C3N4 graphitic form, Journal of Materials Science 35 (2000) 2547–2552, https://doi.org/10.1023/A:1004798509417.
[49] Z. Zhang, K. Leinenweber, M. Bauer, L.A.J. Garvie, P.F. McMillan, G.H. Wolf, High-Pressure Bulk Synthesis of Crystalline C6N9H3·HCl: A Novel C3N4 Graphitic Derivative, J. Am. Chem. Soc. 123 (2001) 7788–7796, https://doi.org/10.1021/ja0103849.
[50] X. Bai, J. Li, C. Cao, Synthesis of hollow carbon nitride microspheres by an electrodeposition method, Applied Surface Science 256 (2010) 2327–2331, https://doi.org/10.1016/j.apsusc.2009.10.061.
[51] A. Thomas, A. Fischer, F. Goettmann, M. Antonietti, J.-O. Müller, R. Schlögl, J. M. Carlsson, Graphitic carbon nitride materials: variation of structure and morphology and their use as metal-free catalysts, J. Mater. Chem. 18 (2008) 4893–4908, https://doi.org/10.1039/B800274F.
[52] S. Zhao, Y. Zhang, Y. Zhou, Y. Wang, K. Qiu, C. Zhang, J. Fang, X. Sheng, Facile one-step synthesis of hollow mesoporous g-C3N4 spheres with ultrathin nanosheets for photoredox water splitting, Carbon 126 (2018) 247–256, https://doi.org/10.1016/j.carbon.2017.10.033.
[53] Q. Li, J. Yang, D. Feng, Z. Wu, Q. Wu, S.S. Park, C.-S. Ha, D. Zhao, Facile synthesis of porous carbon nitride spheres with hierarchical three-dimensional mesostructures for CO2 capture, Nano Res. 3 (2010) 632–642, https://doi.org/10.1007/s12274-010-0023-7.
[54] Q. Gu, Y. Liao, L. Yin, J. Long, X. Wang, C. Xue, Template-free synthesis of porous graphitic carbon nitride microspheres for enhanced photocatalytic hydrogen generation with high stability, Applied Catalysis b: Environmental 165 (2015) 503–510, https://doi.org/10.1016/j.apcatb.2014.10.045.
[55] C. Zhou, C. Lai, D. Huang, G. Zeng, C. Zhang, M. Cheng, L. Hu, J. Wan, W. Xiong, M. Wen, X. Wen, L. Qin, Highly porous carbon nitride by supramolecular preassembly of monomers for photocatalytic removal of sulfamethazine under visible light driven, Applied Catalysis b: Environmental 220 (2018) 202–210, https://doi.org/10.1016/j.apcatb.2017.08.055.
[56] I. Papailias, N. Todorova, T. Giannakopoulou, N. Ioannidis, N. Boukos, C. P. Athanasekou, D. Dimotikali, C. Trapalis, Chemical vs thermal exfoliation of g-C3N4 for NOx removal under visible light irradiation, Applied Catalysis b: Environmental 239 (2018) 16–26, https://doi.org/10.1016/j.apcatb.2018.07.078.
[57] Z. Zhou, Y. Zhang, Y. Shen, S. Liu, Y. Zhang, Molecular engineering of polymeric carbon nitride: advancing applications from photocatalysis to biosensing and more, Chem. Soc. Rev. 47 (2018) 2298–2321, https://doi.org/10.1039/C7CS00840F.
[58] M. Chen, X. Zhao, Y. Li, P. Zeng, H. Liu, H. Yu, M. Wu, Z. Li, D. Shao, C. Miao, G. Chen, H. Shu, Y. Pei, X. Wang, Kinetically elevated redox conversion of polysulfides of lithium-sulfur battery using a separator modified with transition metals coordinated g-C3N4 with carbon-conjugated, Chemical Engineering Journal 385 (2020) 123905, https://doi.org/10.1016/j.cej.2019.123905.
[59] P. Deng, J. Xiong, S. Lei, W. Wang, X. Ou, Y. Xu, Y. Xiao, B. Cheng, Nickel formate induced high-level in situ Ni-doping of g-C3N4 for a tunable band structure and enhanced photocatalytic performance, J. Mater. Chem. A 7 (2019) 22385–22397, https://doi.org/10.1039/C9TA04559G.
[60] M. Xie, J. Tang, L. Kong, W. Lu, V. Natarajan, F. Zhu, J. Zhan, Cobalt doped g-C3N4 activation of peroxymonosulfate for monochlorophenols degradation, Chemical Engineering Journal 360 (2019) 1213–1222, https://doi.org/10.1016/j.cej.2018.10.130.
[61] S.-L. Li, H. Yin, X. Kan, L.-Y. Gan, U. Schwingenschlögl, Y. Zhao, Potential of transition metal atoms embedded in buckled monolayer g-C3N4 as single-atom catalysts, Phys. Chem. Chem. Phys. 19 (2017) 30069–30077, https://doi.org/10.1039/C7CP05195F.
[62] J. Liu, H. He, Z. Shen, H.H. Wang, W. Li, Photoassisted highly efficient activation of persulfate over a single-atom Cu catalyst for tetracycline degradation: Process and mechanism, Journal of Hazardous Materials 429 (2022) 128398, https://doi.org/10.1016/j.jhazmat.2022.128398.
[63] B. Zhu, B. Cheng, L. Zhang, J. Yu, Review on DFT calculation of s-triazine-based carbon nitride, Carbon, Energy 1 (2019) 32–56, https://doi.org/10.1002/cey2.1.
[64] B. Liu, W. Guo, Q. Si, W. Jia, S. Zheng, H. Wang, Q. Zhao, H. Luo, J. Jiang, N. Ren, Atomically dispersed cobalt on carbon nitride for peroxymonosulfate activation: Switchable catalysis enabled by light irradiation, Chemical Engineering Journal 446 (2022) 137277, https://doi.org/10.1016/j.cej.2022.137277.
[65] X. Peng, J. Wu, Z. Zhao, X. Wang, H. Dai, L. Xu, G. Xu, Y. Jian, F. Hu, Activation of peroxymonosulfate by single-atom Fe-g-C3N4 catalysts for high efficiency degradation of tetracycline via nonradical pathways: Role of high-valent iron-oxo species and Fe–Nx sites, Chemical Engineering Journal 427 (2022) 130803, https://doi.org/10.1016/j.cej.2021.130803.
[66] J. Xu, Y. Chen, M. Chen, J. Wang, L. Wang, In situ growth strategy synthesis of single-atom nickel/sulfur co-doped g-C3N4 for efficient photocatalytic tetracycline degradation and CO2 reduction, Chemical Engineering Journal 442 (2022) 136208, https://doi.org/10.1016/j.cej.2022.136208.
[67] R. Zhan, Y. Zhou, C. Liu, X. Wang, X. Sun, Y. Zhu, J. Niu, Insights into mechanism of Fe-dominated active sites via phosphorus bridging in Fe-Ni bimetal single atom photocatalysts, Separation and Purification Technology 286 (2022) 120443, https://doi.org/10.1016/j.seppur.2022.120443.

[68] J. Fu, S. Wang, Z. Wang, K. Liu, H. Li, H. Liu, J. Hu, X. Xu, H. Li, M. Liu, Graphitic carbon nitride based single-atom photocatalysts, Front. Phys. 15 (2020) 33201, https://doi.org/10.1007/s11467-019-0950-z.
[69] H. Fei, J. Dong, M.J. Arellano-Jiménez, G. Ye, N. Dong Kim, E.L.G. Samuel, Z. Peng, Z. Zhu, F. Qin, J. Bao, M.J. Yacaman, P.M. Ajayan, D. Chen, J.M. Tour, Atomic cobalt on nitrogen-doped graphene for hydrogen generation, Nat Commun 6 (2015) 8668, https://doi.org/10.1038/ncomms9668.
[70] G. Vilé, D. Albani, M. Nachtegaal, Z. Chen, D. Dontsova, M. Antonietti, N. López, J. Pérez-Ramírez, A Stable Single-Site Palladium Catalyst for Hydrogenations, Angewandte Chemie International Edition 54 (2015) 11265–11269, https://doi.org/10.1002/anie.201505073.
[71] Z. Zhou, M. Li, C. Kuai, Y. Zhang, V.F. Smith, F. Lin, A. Aiello, D.P. Durkin, H. Chen, D. Shuai, Fe-based single-atom catalysis for oxidizing contaminants of emerging concern by activating peroxides, Journal of Hazardous Materials 418 (2021) 126294, https://doi.org/10.1016/j.jhazmat.2021.126294.
[72] S. Huang, B. Hu, S. Zhao, S. Zhang, M. Wang, Q. Jia, L. He, Z. Zhang, M. Du, Multiple catalytic sites of Fe-N and Fe-N-C single atoms embedded N-doped carbon heterostructures for high-efficiency removal of malachite green, Chemical Engineering Journal 430 (2022) 132933, https://doi.org/10.1016/j.cej.2021.132933.
[73] C. Zhu, Y. Nie, F. Cun, Y. Wang, Z. Tian, F. Liu, Two-step pyrolysis to anchor ultrahigh-density single-atom FeN5 sites on carbon nitride for efficient Fenton-like catalysis near 0 °C, Applied Catalysis b: Environmental 319 (2022) 121900, https://doi.org/10.1016/j.apcatb.2022.121900.
[74] J. Li, Y. Jiang, Q. Wang, C.-Q. Xu, D. Wu, M.N. Banis, K.R. Adair, K. Doyle-Davis, D.M. Meira, Y.Z. Finfrock, W. Li, L. Zhang, T.-K. Sham, R. Li, N. Chen, M. Gu, J. Li, X. Sun, A general strategy for preparing pyrrolic-N4 type single-atom catalysts via pre-located isolated atoms, Nat Commun 12 (2021) 6806, https://doi.org/10.1038/s41467-021-27143-5.
[75] J. Li, S. Zhao, S.-Z. Yang, S. Wang, H. Sun, S.P. Jiang, B. Johannessen, S. Liu, Atomically dispersed cobalt on graphitic carbon nitride as a robust catalyst for selective oxidation of ethylbenzene by peroxymonosulfate, J. Mater. Chem. A 9 (2021) 3029–3035, https://doi.org/10.1039/D0TA11503G.
[76] Q. Wang, C. Liu, D. Zhou, X. Chen, M. Zhang, K. Lin, Degradation of bisphenol a using peroxymonosulfate activated by single-atomic cobalt catalysts: Different reactive species at acidic and alkaline pH, Chemical Engineering Journal 439 (2022) 135002, https://doi.org/10.1016/j.cej.2022.135002.
[77] T. Li, P. Cui, X. Wang, C. Liu, Y. Zeng, G. Fang, Y. Zhao, J. Gao, Y. Wang, D. Zhou, Efficient activation of peroxymonosulfate by $C_{3N}5$ doped with cobalt for organic contaminant degradation, Environ. Sci.: Nano 9 (2022) 2534–2547, https://doi.org/10.1039/D2EN00216G.
[78] Y. Zhou, W. Qin, X. Sun, Y. Zhu, J. Niu, Synergistic effects on d-band center via coordination sites of M-N3P1 (M = Co and Ni) in dual single atoms that enhances photocatalytic dechlorination from tetrachlorobispheonl A, J. Hazard. Mater. 430 (2022) 128419, https://doi.org/10.1016/j.jhazmat.2022.128419.
[79] S. Wang, J. Wang, Single atom cobalt catalyst derived from co-pyrolysis of vitamin B12 and graphitic carbon nitride for PMS activation to degrade emerging pollutants, Applied Catalysis b: Environmental 321 (2023) 122051, https://doi.org/10.1016/j.apcatb.2022.122051.
[80] L. Cao, Q. Luo, W. Liu, Y. Lin, X. Liu, Y. Cao, W. Zhang, Y. Wu, J. Yang, T. Yao, S. Wei, Identification of single-atom active sites in carbon-based cobalt catalysts during electrocatalytic hydrogen evolution, Nat Catal 2 (2018) 134–141, https://doi.org/10.1038/s41929-018-0203-5.
[81] L. Lyu, L. Zhang, Q. Wang, Y. Nie, C. Hu, Enhanced Fenton Catalytic Efficiency of γ-Cu–Al2O3 by σ-Cu2+–Ligand Complexes from Aromatic Pollutant Degradation, Environ. Sci. Technol. 49 (2015) 8639–8647, https://doi.org/10.1021/acs.est.5b00445.
[82] J. Xu, X. Zheng, Z. Feng, Z. Lu, Z. Zhang, W. Huang, Y. Li, D. Vuckovic, Y. Li, S. Dai, G. Chen, K. Wang, H. Wang, J.K. Chen, W. Mitch, Y. Cui, Organic wastewater treatment by a single-atom catalyst and electrolytically produced H2O2, Nat Sustain 4 (2020) 233–241, https://doi.org/10.1038/s41893-020-00635-w.
[83] C. Cometto, A. Ugolotti, E. Grazietti, A. Moretto, G. Bottaro, L. Armelao, C. Di Valentin, L. Calvillo, G. Granozzi, Copper single-atoms embedded in 2D graphitic carbon nitride for the CO2 reduction, Npj 2D Mater Appl 5 (2021) 63. https://doi.org/10.1038/s41699-021-00243-y.
[84] F. Chen, X.-L. Wu, L. Yang, C. Chen, H. Lin, J. Chen, Efficient degradation and mineralization of antibiotics via heterogeneous activation of peroxymonosulfate by using graphene supported single-atom Cu catalyst, Chemical Engineering Journal 394 (2020) 124904, https://doi.org/10.1016/j.cej.2020.124904.
[85] X. Chang, S. Xu, D. Wang, Z. Zhang, Y. Guo, S. Kang, Flash dual-engineering of surface carboxyl defects and single Cu atoms of g-C3N4 via unique CO2 plasma immersion approach for boosted photocatalytic activity, Materials Today Advances 15 (2022) 100274, https://doi.org/10.1016/j.mtadv.2022.100274.
[86] Y. Liu, L. Xu, N. Zhang, J. Wang, X. Mu, Y. Wang, A promoted charge separation/transfer and surface plasmon resonance effect synergistically enhanced photocatalytic performance in Cu nanoparticles and single-atom Cu supported attapulgite/polymer carbon nitride photocatalyst, Materials Today Chemistry 26 (2022) 101250, https://doi.org/10.1016/j.mtchem.2022.101250.
[87] G. Wang, R. Huang, J. Zhang, J. Mao, D. Wang, Y. Li, Synergistic Modulation of the Separation of Photo-Generated Carriers via Engineering of Dual Atomic Sites for Promoting Photocatalytic Performance, Advanced Materials 33 (2021) 2105904, https://doi.org/10.1002/adma.202105904.
[88] X. Liu, F. He, Y. Lu, S. Wang, C. Zhao, S. Wang, X. Duan, H. Zhang, X. Zhao, H. Sun, J. Zhang, S. Wang, The double-edged effect of single atom metals on photocatalysis, Chemical Engineering Journal 453 (2023) 139833.
[89] Y. Hou, M. Qiu, M.G. Kim, P. Liu, G. Nam, T. Zhang, X. Zhuang, B. Yang, J. Cho, M. Chen, C. Yuan, L. Lei, X. Feng, Atomically dispersed nickel–nitrogen–sulfur species anchored on porous carbon nanosheets for efficient water oxidation, Nat Commun 10 (2019) 1392, https://doi.org/10.1038/s41467-019-09394-5.
[90] Q. Wang, K. Liu, K. Hu, C. Cai, H. Li, H. Li, M. Herran, Y.-R. Lu, T.-S. Chan, C. Ma, J. Fu, S. Zhang, Y. Liang, E. Cortés, M. Liu, Attenuating metal-substrate conjugation in atomically dispersed nickel catalysts for electroreduction of CO2 to CO, Nat Commun 13 (2022) 6082, https://doi.org/10.1038/s41467-022-33692-0.
[91] X. Hai, S. Xi, S. Mitchell, K. Harrath, H. Xu, D.F. Akl, D. Kong, J. Li, Z. Li, T. Sun, H. Yang, Y. Cui, C. Su, X. Zhao, J. Li, J. Pérez-Ramírez, J. Lu, Scalable two-step annealing method for preparing ultra-high-density single-atom catalyst libraries, Nat. Nanotechnol. 17 (2022) 174–181, https://doi.org/10.1038/s41565-021-01022-y.
[92] J. Yang, D. Zeng, Q. Zhang, R. Cui, M. Hassan, L. Dong, J. Li, Y. He, Single Mn atom anchored on N-doped porous carbon as highly efficient Fenton-like catalyst for the degradation of organic contaminants, Applied Catalysis b: Environmental 279 (2020) 119363, https://doi.org/10.1016/j.apcatb.2020.119363.
[93] J. Miao, J. Song, J. Lang, Y. Zhu, J. Dai, Y. Wei, M. Long, Z. Shao, B. Zhou, P.J. J. Alvarez, L. Zhang, Single-Atom MnN 5 Catalytic Sites Enable Efficient Peroxymonosulfate Activation by Forming Highly Reactive Mn(IV)–Oxo Species, Environ. Sci. Technol. 57 (2023) 4266–4275, https://doi.org/10.1021/acs.est.2c08836.
[94] Z. Wang, Y. Zhang, Y. Yu, M. Jia, X. Tao, Promoting photocatalytic degradation of tetracycline over in-situ grown single manganese atoms on polymeric carbon nitride, Applied Surface Science 593 (2022) 153458, https://doi.org/10.1016/j.apsusc.2022.153458.
[95] F. Chen, X. Wu, C. Shi, H. Lin, J. Chen, Y. Shi, S. Wang, X. Duan, Molecular Engineering toward Pyrrolic N-Rich M-N 4 (M = Cr, Mn, Fe Co, Cu) Single-Atom Sites for Enhanced Heterogeneous Fenton-Like Reaction, Adv. Funct. Mater. 31 (2021) 2007877, https://doi.org/10.1002/adfm.202007877.
[96] Z. Li, H. He, H. Cao, S. Sun, W. Diao, D. Gao, P. Lu, S. Zhang, Z. Guo, M. Li, R. Liu, D. Ren, C. Liu, Y. Zhang, Z. Yang, J. Jiang, G. Zhang, Atomic Co/Ni dual sites and Co/Ni alloy nanoparticles in N-doped porous Janus-like carbon frameworks for bifunctional oxygen electrocatalysis, Applied Catalysis b: Environmental 240 (2019) 112–121, https://doi.org/10.1016/j.apcatb.2018.08.074.
[97] C. Han, X. Bo, J. Liu, M. Li, M. Zhou, L. Guo, Fe, Co bimetal activated N-doped graphitic carbon layers as noble metal-free electrocatalysts for high-performance oxygen reduction reaction, Journal of Alloys and Compounds 710 (2017) 57–65, https://doi.org/10.1016/j.jallcom.2017.03.241.
[98] L. Bai, C.-S. Hsu, D.T.L. Alexander, H.M. Chen, X. Hu, Double-atom catalysts as a molecular platform for heterogeneous oxygen evolution electrocatalysis, Nat Energy 6 (2021) 1054–1066, https://doi.org/10.1038/s41560-021-00925-3.
[99] Q. Hao, H. Zhong, J. Wang, K. Liu, J. Yan, Z. Ren, N. Zhou, X. Zhao, H. Zhang, D. Liu, X. Liu, L. Chen, J. Luo, X. Zhang, Nickel dual-atom sites for electrochemical carbon dioxide reduction, Nat. Synth 1 (2022) 719–728, https://doi.org/10.1038/s44160-022-00138-w.
[100] X. Guo, J. Gu, S. Lin, S. Zhang, Z. Chen, S. Huang, Tackling the Activity and Selectivity Challenges of Electrocatalysts toward the Nitrogen Reduction Reaction via Atomically Dispersed Biatom Catalysts, J. Am. Chem. Soc. 142 (2020) 5709–5721, https://doi.org/10.1021/jacs.9b13349.
[101] S. Zhang, Y. Wu, Y.-X. Zhang, Z. Niu, Dual-atom catalysts: controllable synthesis and electrocatalytic applications, Sci. China Chem. 64 (2021) 1908–1922, https://doi.org/10.1007/s11426-021-1106-9.
[102] L. Zhang, R. Si, H. Liu, N. Chen, Q. Wang, K. Adair, Z. Wang, J. Chen, Z. Song, J. Li, M.N. Banis, R. Li, T.-K. Sham, M. Gu, L.-M. Liu, G.A. Botton, X. Sun, Atomic layer deposited Pt-Ru dual-metal dimers and identifying their active sites for hydrogen evolution reaction, Nat Commun 10 (2019) 4936, https://doi.org/10.1038/s41467-019-12887-y.
[103] S. Tian, Q. Fu, W. Chen, Q. Feng, Z. Chen, J. Zhang, W.-C. Cheong, R. Yu, L. Gu, J. Dong, J. Luo, C. Chen, Q. Peng, C. Draxl, D. Wang, Y. Li, Carbon nitride supported Fe2 cluster catalysts with superior performance for alkene epoxidation, Nat Commun 9 (2018) 2353, https://doi.org/10.1038/s41467-018-04845-x.
[104] W. Ye, S. Chen, Y. Lin, L. Yang, S. Chen, X. Zheng, Z. Qi, C. Wang, R. Long, M. Chen, J. Zhu, P. Gao, L. Song, J. Jiang, Y. Xiong, Precisely Tuning the Number of Fe Atoms in Clusters on N-Doped Carbon toward Acidic Oxygen Reduction Reaction, Chem 5 (2019) 2865–2878, https://doi.org/10.1016/j.chempr.2019.07.020.
[105] Z. Zeng, L.Y. Gan, H. Bin Yang, X. Su, J. Gao, W. Liu, H. Matsumoto, J. Gong, J. Zhang, W. Cai, Z. Zhang, Y. Yan, B. Liu, P. Chen, Orbital coupling of hetero-diatomic nickel-iron site for bifunctional electrocatalysis of CO2 reduction and oxygen evolution, Nat Commun 12 (2021) 4088, https://doi.org/10.1038/s41467-021-24052-5.
[106] D. Yao, C. Tang, X. Zhi, B. Johannessen, A. Slattery, S. Chern, S. Qiao, Inter-Metal Interaction with a Threshold Effect in NiCu Dual-Atom Catalysts for CO 2 Electroreduction, Advanced Materials 35 (2023) 2209386, https://doi.org/10.1002/adma.202209386.
[107] W. Wan, Y. Zhao, S. Wei, C.A. Triana, J. Li, A. Arcifa, C.S. Allen, R. Cao, G. R. Patzke, Mechanistic insight into the active centers of single/dual-atom Ni/Fe-based oxygen electrocatalysts, Nat Commun 12 (2021) 5589, https://doi.org/10.1038/s41467-021-25811-0.
[108] G. Yang, J. Zhu, P. Yuan, Y. Hu, G. Qu, B.-A. Lu, X. Xue, H. Yin, W. Cheng, J. Cheng, W. Xu, J. Li, J. Hu, S. Mu, J.-N. Zhang, Regulating Fe-spin state by atomically dispersed Mn-N in Fe-N-C catalysts with high oxygen reduction activity, Nat Commun 12 (2021) 1734, https://doi.org/10.1038/s41467-021-21919-5.

[109] Y. Zhou, M. Yu, Q. Zhang, X. Sun, J. Niu, Regulating electron distribution of Fe/Ni-N4P2 single sites for efficient photo-Fenton process, Journal of Hazardous Materials 440 (2022) 129724, https://doi.org/10.1016/j.jhazmat.2022.129724.
[110] M. Yu, C. Liu, X. Sun, J. Lu, J. Niu, Understanding of the Dual Roles of Phosphorus in Atomically Distributed Fe/Co-N $_{4\ P}$ 2 over Carbon Nitride for Photocatalytic Debromination from Tetrabromobisphenol A, ACS Appl. Mater. Interfaces 14 (2022) 5376–5383, https://doi.org/10.1021/acsami.1c21850.
[111] Y. Gao, Y. Zhu, L. Lyu, Q. Zeng, X. Xing, C. Hu, Electronic Structure Modulation of Graphitic Carbon Nitride by Oxygen Doping for Enhanced Catalytic Degradation of Organic Pollutants through Peroxymonosulfate Activation, Environ. Sci. Technol. 52 (2018) 14371–14380, https://doi.org/10.1021/acs.est.8b05246.
[112] S. Wang, Y. Liu, J. Wang, Peroxymonosulfate Activation by Fe–Co–O-Codoped Graphite Carbon Nitride for Degradation of Sulfamethoxazole, Environ. Sci. Technol. 54 (2020) 10361–10369, https://doi.org/10.1021/acs.est.0c03256.
[113] W. Wu, Z. Ruan, J. Li, Y. Li, Y. Jiang, X. Xu, D. Li, Y. Yuan, K. Lin, In Situ Preparation and Analysis of Bimetal Co-doped Mesoporous Graphitic Carbon Nitride with Enhanced Photocatalytic Activity, Nano-Micro Lett. 11 (2019) 10, https://doi.org/10.1007/s40820-018-0236-y.
[114] J. Wang, Y. Song, C. Zuo, R. Li, Y. Zhou, Y. Zhang, B. Wu, Few-layer porous carbon nitride anchoring Co and Ni with charge transfer mechanism for photocatalytic CO2 reduction, Journal of Colloid and Interface Science 625 (2022) 722–733, https://doi.org/10.1016/j.jcis.2022.04.153.
[115] Z. Zhao, M. Hu, T. Nie, W. Zhou, B. Pan, B. Xing, L. Zhu, Improved Electronic Structure from Spin-State Reconstruction of a Heteronuclear Fe–Co Diatomic Pair to Boost the Fenton-like Reaction, Environ. Sci. Technol. 57 (2023) 4556–4567, https://doi.org/10.1021/acs.est.2c09336.
[116] J. Shan, C. Ye, C. Zhu, J. Dong, W. Xu, L. Chen, Y. Jiao, Y. Jiang, L. Song, Y. Zhang, M. Jaroniec, Y. Zhu, Y. Zheng, S.-Z. Qiao, Integrating Interactive Noble Metal Single-Atom Catalysts into Transition Metal Oxide Lattices, J. Am. Chem. Soc. 144 (2022) 23214–23222, https://doi.org/10.1021/jacs.2c11374.
[117] L. Cheng, X. Yue, L. Wang, D. Zhang, P. Zhang, J. Fan, Q. Xiang, Dual-Single-Atom Tailoring with Bifunctional Integration for High-Performance CO2 Photoreduction, Advanced Materials 33 (2021) 2105135, https://doi.org/10.1002/adma.202105135.
[118] I. Ro, J. Qi, S. Lee, M. Xu, X. Yan, Z. Xie, G. Zakem, A. Morales, J.G. Chen, X. Pan, D.G. Vlachos, S. Caratzoulas, P. Christopher, Bifunctional hydroformylation on heterogeneous Rh-WOx pair site catalysts, Nature 609 (2022) 287–292, https://doi.org/10.1038/s41586-022-05075-4.
[119] P. Xie, J. Ding, Z. Yao, T. Pu, P. Zhang, Z. Huang, C. Wang, J. Zhang, N. Zecher-Freeman, H. Zong, D. Yuan, S. Deng, R. Shahbazian-Yassar, C. Wang, Oxo dicopper anchored on carbon nitride for selective oxidation of methane, Nat Commun 13 (2022) 1375, https://doi.org/10.1038/s41467-022-28987-1.
[120] M.J. Hülsey, B. Zhang, Z. Ma, H. Asakura, D.A. Do, W. Chen, T. Tanaka, P. Zhang, Z. Wu, N. Yan, In situ spectroscopy-guided engineering of rhodium single-atom catalysts for CO oxidation, Nat Commun 10 (2019) 1330, https://doi.org/10.1038/s41467-019-09188-9.
[121] J. Miao J. Song J. Lang Y. Zhu J. Dai Y. Wei M. Long Z. Shao B. Zhou P.J.J. Alvarez L. Zhang Single-Atom MnN 5 Catalytic Sites Enable Efficient Peroxymonosulfate Activation by Forming Highly Reactive Mn(IV)–Oxo Species Environ. Sci. Technol. 2023 acs.est.2c08836 10.1021/acs.est.2c08836.
[122] Q. Zhang, J. Guan, Single-Atom Catalysts for Electrocatalytic Applications, Advanced Functional Materials 30 (2020) 2000768, https://doi.org/10.1002/adfm.202000768.
[123] G. Wang, X. Nie, X. Ji, X. Quan, S. Chen, H. Wang, H. Yu, X. Guo, Enhanced heterogeneous activation of peroxymonosulfate by Co and N codoped porous carbon for degradation of organic pollutants: the synergism between Co and N, Environ. Sci.: Nano 6 (2019) 399–410, https://doi.org/10.1039/C8EN01231H.
[124] S. An, G. Zhang, T. Wang, W. Zhang, K. Li, C. Song, J.T. Miller, S. Miao, J. Wang, X. Guo, High-Density Ultra-small Clusters and Single-Atom Fe Sites Embedded in Graphitic Carbon Nitride (g-C3N4) for Highly Efficient Catalytic Advanced Oxidation Processes, ACS Nano 12 (2018) 9441–9450, https://doi.org/10.1021/acsnano.8b04693.
[125] F. Wang, Y. Wang, Y. Feng, Y. Zeng, Z. Xie, Q. Zhang, Y. Su, P. Chen, Y. Liu, K. Yao, W. Lv, G. Liu, Novel ternary photocatalyst of single atom-dispersed silver and carbon quantum dots co-loaded with ultrathin g-C3N4 for broad spectrum photocatalytic degradation of naproxen, Applied Catalysis b: Environmental 221 (2018) 510–520, https://doi.org/10.1016/j.apcatb.2017.09.055.
[126] M. Qian, X. Wu, M. Lu, L. Huang, W. Li, H. Lin, J. Chen, S. Wang, X. Duan, Modulation of Charge Trapping by Island-like Single-Atom Cobalt Catalyst for Enhanced Photo-Fenton-Like reaction, Adv Funct Materials 33 (2023) 2208688, https://doi.org/10.1002/adfm.202208688.
[127] S. Dong, X. Chen, L. Su, Y. Wen, Y. Wang, Q. Yang, L. Yi, W. Xu, Q. Yang, P. He, Y. Zhu, Z. Lu, Integration of Atomically Dispersed Cu–N $_4$ Sites with C $_{3\ N}$ 4 for Enhanced Photo-Fenton Degradation over a Nonradical Mechanism, ACS EST Eng. 3 (2023) 150–164, https://doi.org/10.1021/acsestengg.2c00261.
[128] C. Han, R. Qi, R. Sun, K. Fan, B. Johannessen, D.-C. Qi, S. Cao, J. Xu, Enhanced support effects in single-atom copper-incorporated carbon nitride for photocatalytic suzuki cross-coupling reactions, Applied Catalysis b: Environmental 320 (2023) 121954, https://doi.org/10.1016/j.apcatb.2022.121954.
[129] M. Liu, H. Xia, W. Yang, X. Liu, J. Xiang, X. Wang, L. Hu, F. Lu, Novel Cu-Fe bi-metal oxide quantum dots coupled g-C3N4 nanosheets with H2O2 adsorption-activation trade-off for efficient photo-Fenton catalysis, Applied Catalysis b: Environmental 301 (2022) 120765, https://doi.org/10.1016/j.apcatb.2021.120765.
[130] L. Su, P. Wang, X. Ma, J. Wang, S. Zhan, Regulating Local Electron Density of Iron Single Sites by Introducing Nitrogen Vacancies for Efficient Photo-Fenton Process, Angewandte Chemie International Edition 60 (2021) 21261–21266, https://doi.org/10.1002/anie.202108937.
[131] S. Mao, C. Liu, Y. Wu, M. Xia, F. Wang, Porous P, Fe-doped g-C3N4 nanostructure with enhanced photo-Fenton activity for removal of tetracycline hydrochloride: Mechanism insight, DFT Calculation and Degradation Pathways, Chemosphere 291 (2022) 133039, https://doi.org/10.1016/j.chemosphere.2021.133039.
[132] G. Zhao, W. Li, H. Zhang, W. Wang, Y. Ren, Single atom Fe-dispersed graphitic carbon nitride (g-C3N4) as a highly efficient peroxymonosulfate photocatalytic activator for sulfamethoxazole degradation, Chemical Engineering Journal 430 (2022) 132937, https://doi.org/10.1016/j.cej.2021.132937.
[133] W.-D. Oh, Z. Dong, T.-T. Lim, Generation of sulfate radical through heterogeneous catalysis for organic contaminants removal: Current development, challenges and prospects, Applied Catalysis b: Environmental 194 (2016) 169–201, https://doi.org/10.1016/j.apcatb.2016.04.003.
[134] X. Duan, H. Sun, S. Wang, Metal-Free Carbocatalysis in Advanced Oxidation Reactions, Acc. Chem. Res. 51 (2018) 678–687, https://doi.org/10.1021/acs.accounts.7b00535.
[135] L. Zhang, X. Jiang, Z. Zhong, L. Tian, Q. Sun, Y. Cui, X. Lu, J. Zou, S. Luo, Carbon Nitride Supported High-Loading Fe Single-Atom Catalyst for Activation of Peroxymonosulfate to Generate 1 O 2 with 100 % Selectivity, Angew Chem Int Ed 60 (2021) 21751–21755, https://doi.org/10.1002/anie.202109488.
[136] S. Zhu, X. Li, J. Kang, X. Duan, S. Wang, Persulfate Activation on Crystallographic Manganese Oxides: Mechanism of Singlet Oxygen Evolution for Nonradical Selective Degradation of Aqueous Contaminants, Environ. Sci. Technol. 53 (2019) 307–315, https://doi.org/10.1021/acs.est.8b04669.
[137] J. Lee, S. Hong, Y. Mackeyev, C. Lee, E. Chung, L.J. Wilson, J.-H. Kim, P.J. J. Alvarez, Photosensitized Oxidation of Emerging Organic Pollutants by Tetrakis $_C$ 60 Aminofullerene-Derivatized Silica under Visible Light Irradiation, Environ. Sci. Technol. 45 (2011) 10598–10604, https://doi.org/10.1021/es2029944.
[138] X. Liang, D. Wang, Z. Zhao, T. Li, Y. Gao, C. Hu, Coordination Number Dependent Catalytic Activity of Single-Atom Cobalt Catalysts for Fenton-Like Reaction, Adv Funct Materials 32 (2022) 2203001, https://doi.org/10.1002/adfm.202203001.
[139] Z. Wang, E. Almatrafi, H. Wang, H. Qin, W. Wang, L. Du, S. Chen, G. Zeng, P. Xu, Cobalt Single Atoms Anchored on Oxygen-Doped Tubular Carbon Nitride for Efficient Peroxymonosulfate Activation: Simultaneous Coordination Structure and Morphology Modulation, Angewandte Chemie 134 (2022) e202202338.
[140] C. Wan, X. Duan, Y. Huang, Molecular Design of Single-Atom Catalysts for Oxygen Reduction Reaction, Advanced Energy Materials 10 (2020) 1903815, https://doi.org/10.1002/aenm.201903815.
[141] Y. Pan, R. Lin, Y. Chen, S. Liu, W. Zhu, X. Cao, W. Chen, K. Wu, W.-C. Cheong, Y. Wang, L. Zheng, J. Luo, Y. Lin, Y. Liu, C. Liu, J. Li, Q. Lu, X. Chen, D. Wang, Q. Peng, C. Chen, Y. Li, Design of Single-Atom Co–N $_5$ Catalytic Site: A Robust Electrocatalyst for CO $_2$ Reduction with Nearly 100% CO Selectivity and Remarkable Stability, J. Am. Chem. Soc. 140 (2018) 4218–4221, https://doi.org/10.1021/jacs.8b00814.
[142] Y. Wang, X. Hu, J. Hao, R. Ma, Q. Guo, H. Gao, H. Bai, Nitrogen and Oxygen Codoped Porous Carbon with Superior CO $_2$ Adsorption Performance: A Combined Experimental and DFT Calculation Study, Ind. Eng. Chem. Res. 58 (2019) 13390–13400, https://doi.org/10.1021/acs.iecr.9b01454.
[143] S. Wacławek, H.V. Lutze, K. Grübel, V.V.T. Padil, M. Černík, D. Dionysios, Dionysiou, Chemistry of persulfates in water and wastewater treatment: A review, Chemical Engineering Journal 330 (2017) 44–62, https://doi.org/10.1016/j.cej.2017.07.132.
[144] Q. Wang, D. Zhou, C. Liu, X. Chen, L. Liu, K. Lin, Enhancing effect of dual-atom catalysts on tetrabromobisphenol S degradation via peroxydisulfate activation: Synergism of Fe–Cu and electron-transfer mechanism, Chemical Engineering Journal 460 (2023) 140681, https://doi.org/10.1016/j.cej.2022.140681.
[145] H. Wu, J. Yan, X. Xu, Q. Yuan, J. Wang, J. Cui, A. Lin, Synergistic effects for boosted persulfate activation in a designed Fe–Cu dual-atom site catalyst, Chemical Engineering Journal 428 (2022) 132611, https://doi.org/10.1016/j.cej.2021.132611.
[146] Z. Guo, Y. Xie, J. Xiao, Z.-J. Zhao, Y. Wang, Z. Xu, Y. Zhang, L. Yin, H. Cao, J. Gong, Single-Atom Mn–N4 Site-Catalyzed Peroxone Reaction for the Efficient Production of Hydroxyl Radicals in an Acidic Solution, J. Am. Chem. Soc. 141 (2019) 12005–12010, https://doi.org/10.1021/jacs.9b04569.
[147] Z. Guo, Y. Xie, J. Xiao, Z.-J. Zhao, Y. Wang, Z. Xu, Y. Zhang, L. Yin, H. Cao, J. Gong, Single-Atom Mn–N $_4$ Site-Catalyzed Peroxone Reaction for the Efficient Production of Hydroxyl Radicals in an Acidic Solution, J. Am. Chem. Soc. 141 (2019) 12005–12010, https://doi.org/10.1021/jacs.9b04569.
[148] R. Li, D. Wang, Superiority of Dual-Atom Catalysts in Electrocatalysis: One Step Further Than Single-Atom Catalysts, Advanced Energy Materials 12 (2022) 2103564, https://doi.org/10.1002/aenm.202103564.
[149] X. Zhao, Z.H. Levell, S. Yu, Y. Liu, Atomistic Understanding of Two-dimensional Electrocatalysts from First Principles, Chem. Rev. 122 (2022) 10675–10709, https://doi.org/10.1021/acs.chemrev.1c00981.
[150] N. Li, X. Song, L. Wang, X. Geng, H. Wang, H. Tang, Z. Bian, Single-Atom Cobalt Catalysts for Electrocatalytic Hydrodechlorination and Oxygen Reduction Reaction for the Degradation of Chlorinated Organic Compounds, ACS Appl. Mater. Interfaces 12 (2020) 24019–24029, https://doi.org/10.1021/acsami.0c05159.
[151] D. Guo, Z. Huang, Y. Liu, Q. Zhang, Y. Yang, J. Hong, Incorporation of single-atom copper into nitrogen-doped graphene for acetaminophen electrocatalytic degradation, Applied Surface Science 604 (2022) 154561, https://doi.org/10.1016/j.apsusc.2022.154561.

[152] D. Zhang, H. Zhang, Y. Du, H. Tang, Y. Tang, Y. Chen, Z. Wang, X. Sun, C. Liu, Highly efficient production of hydroxyl radicals from oxygen reduction over Ni-Fe dual atom electrocatalysts for removing emerging contaminants in wastewater, Chemical Engineering Science 278 (2023) 118914, https://doi.org/10.1016/j.ces.2023.118914.

[153] T. Xiang, Y. Liang, Y. Zeng, J. Deng, J. Yuan, W. Xiong, B. Song, C. Zhou, Y. Yang, Transition Metal Single-Atom Catalysts for the Electrocatalytic Nitrate Reduction: Mechanism, Synthesis, Characterization, Application, and Prospects, Small 19 (2023) 2303732, https://doi.org/10.1002/smll.202303732.

[154] J. Li, M. Li, N. An, S. Zhang, Q. Song, Y. Yang, X. Liu, Atomically dispersed Fe atoms anchored on S and N–codoped carbon for efficient electrochemical denitrification, Proceedings of the National Academy of Sciences 118 (2021) e2105628118. https://doi.org/10.1073/pnas.2105628118.

[155] Z. Liang, C. Peng, J. Shen, Y. Yang, S. Yao, D. Xue, M. Zhu, J. Liu, Lithiophilic single-atom Co on carbon nanosheets synergistically modulates Li deposition enable dendrite-free lithium metal batteries, Journal of Power Sources 556 (2023) 232474, https://doi.org/10.1016/j.jpowsour.2022.232474.

[156] S. Yao, Y. Yang, Z. Liang, J. Chen, J. Ding, F. Li, J. Liu, L. Xi, M. Zhu, J. Liu, A Dual−Functional Cationic Covalent Organic Frameworks Modified Separator for High Energy Lithium Metal Batteries, Advanced Functional Materials 33 (2023) 2212466, https://doi.org/10.1002/adfm.202212466.

[157] H. Kim, J. Lee, H. Ahn, O. Kim, M.J. Park, Synthesis of three-dimensionally interconnected sulfur-rich polymers for cathode materials of high-rate lithium–sulfur batteries, Nat Commun 6 (2015) 7278, https://doi.org/10.1038/ncomms8278.

[158] Z. Wang, H. Che, W. Lu, Y. Chao, L. Wang, B. Liang, J. Liu, Q. Xu, X. Cui, Application of Inorganic Quantum Dots in Advanced Lithium-Sulfur Batteries, Advanced Science 10 (2023) 2301355, https://doi.org/10.1002/advs.202301355.

[159] Z. Wang, J. Shen, X. Xu, J. Yuan, S. Zuo, Z. Liu, D. Zhang, J. Liu, In-Situ Synthesis of Carbon-Encapsulated Atomic Cobalt as Highly Efficient Polysulfide Electrocatalysts for Highly Stable Lithium-Sulfur Batteries, Small 18 (2022) 2106640, https://doi.org/10.1002/smll.202106640.

[160] S. An, G. Zhang, T. Wang, W. Zhang, K. Li, C. Song, J.T. Miller, S. Miao, J. Wang, X. Guo, High-Density Ultra-small Clusters and Single-Atom Fe Sites Embedded in Graphitic Carbon Nitride (g-C 3 N 4) for Highly Efficient Catalytic Advanced Oxidation Processes, ACS Nano 12 (2018) 9441–9450, https://doi.org/10.1021/acsnano.8b04693.

[161] Y. Mao, P. Wang, D. Zhang, Y. Xia, Y. Li, W. Zeng, S. Zhan, J.C. Crittenden, Accelerating Fe ^{III} -Aqua Complex Reduction in an Efficient Solid–Liquid-Interfacial Fenton Reaction over the Mn–CNH Co-catalyst at Near-Neutral pH, Environ. Sci. Technol. (2021), https://doi.org/10.1021/acs.est.1c04534.

[162] S. Zuo, X. Jin, X. Wang, Y. Lu, Q. Zhu, J. Wang, W. Liu, Y. Du, J. Wang, Sandwich structure stabilized atomic Fe catalyst for highly efficient Fenton-like reaction at all pH values, Applied Catalysis b: Environmental 282 (2021) 119551, https://doi.org/10.1016/j.apcatb.2020.119551.

[163] Y. Shang, X. Liu, Y. Li, Y. Gao, B. Gao, X. Xu, Q. Yue, Boosting fenton-like reaction by reconstructed single Fe atom catalyst for oxidizing organics: Synergistic effect of conjugated π-π sp2 structured carbon and isolated Fe-N4 sites, Chemical Engineering Journal 446 (2022) 137120, https://doi.org/10.1016/j.cej.2022.137120.